Available online at www.sciencedirect.com

ScienceDirect

Advances in Space Research 72 (2023) 2801–2823

ADVANCES IN SPACE RESEARCH (a COSPAR publication)

www.elsevier.com/locate/asr

Trajectory optimization for multi-target Active Debris Removal missions

Laura Medioni [a,*], Yvan Gary [b], Myrtille Monclin [b], Côme Oosterhof [b], Gaetan Pierre [b], Tom Semblanet [b], Perrine Comte [a], Kévin Nocentini [a]

[a] Capgemini Engineering, 4 All. des Cormorans, Cannes 06150, France
[b] ISAE-Supaéro, 10 Av. Edouard Belin, Toulouse 31400, France

Received 30 March 2022; received in revised form 2 December 2022; accepted 6 December 2022
Available online 13 December 2022

Abstract

The proliferation of debris in Low Earth Orbit raises increasing challenges about the sustainability of the space environment. The current international recommendations to deorbit satellites at the end of their life are not sufficient to ensure this sustainability. To accelerate the process, it would be necessary to remove hazardous debris and thus de-congest the high-risk orbits. However, active debris removal missions are very expensive, and still in their early stages. One way to reduce its costs is to remove several pieces of debris per removal mission, which corresponds to a global optimization problem, with the objective of optimizing the number of debris removed while minimizing the cost in mission time and in propellant.

In our study, the trajectory optimization is performed using a simulated annealing algorithm. The tool classifies the targets in groups gathered by similarities of orbital parameters, with the objective for each mission not to exceed a total $\Delta V = 4$ km/s for a mission time lower than 3 years. To achieve this, a weighting is made between out-of-plane maneuvers, costly in propellant, and the use of the orbital parameter Ω drift, costly in time, to allow the spacecraft to pass from one debris to another. A criterion is set up to determine from which threshold it is more interesting to carry out a maneuver on Ω rather than to let the gravitational drift act. As a result, applied on the 50 most hazardous debris established by the International Astronautical Federation, we obtain a classification of the 50 pieces of debris into 11 optimal groups, with an average ΔV of 3.05 km/s and an average mission time of 1.5 years, which corresponds to the imposed criteria and validates the feasibility of such ADR missions.

Keywords: Active Debris Removal; GTOC9; Trajectory optimization; Simulated Annealing algorithm; Debris mitigation

1. Introduction

Since the first artificial satellite Sputnik was placed into orbit by the USSR in October 1957, most of the satellites and second stages of launchers sent into space have become debris. The most used orbits, in particular the Low Earth Orbit (LEO), are thus more and more congested, which causes several problems. First of all, space debris in LEO can have relative speeds up to 10 km/s and therefore store a significant kinetic energy: any collision with an active satellite would damage it irreparably, which implies costly avoidance maneuvers (Merz et al., 2017). Moreover, collisions are likely to generate new debris, further increasing orbit congestion and the risk of collision. The possibility of a chain reaction prohibiting all access to space was predicted as early as 1978 by Donald J. Kessler, known as the Kessler syndrome (Kessler and Cour-Palais, 1978).

Currently, the development of mega constellations of satellites in LEO, such as Starlink, as well as the anti-

* Corresponding author.
E-mail address: laura.medioni@capgemini.com (L. Medioni).

https://doi.org/10.1016/j.asr.2022.12.013
0273-1177/

Nomenclature

Acronyms

ADR	Active Debris Removal
ACO	Ant Colony Optimization
ADRIOS	Active Debris Removal and In-Orbit Servicing
ESA	European Space Agency
GA	Genetic Algorithm
GEO	Geostationnary Orbit
GNC	Guidance, Navigation, Control
IOS	In-Orbit Servicing
LEO	Low Earth Orbit
LOS	Loi sur les Opérations Spatiales
MEO	Medium Earth Orbit
TRL	Technical Readiness Level
TSP	Travelling Salesman Problem
RAAN	Right Ascension of Ascending Node
SA	Simulated Annealing
SSO	Sun-Synchronous Orbit
VRP	Vehicle Routing Problem

Variable nomenclature

Algorithm

Control temperature parameter T
Cost function $E(X)$
Iteration parameters t_{iter}, α
Order of magnitude tolerated for a mission in ΔV,*km/s* and Δt, *days* V_{tol}, t_{tol}
State of the system to be optimize X
Total number of debris to remove N_{deb}

Orbital mechanics

Argument of Perigee ° ω
Duration increment days Δt
Cartesian coordinates of spacecraft km (x, y, z)
Earth flatness geopotential term - J_2
Earth Gravitationnal constant m^3/s^2 μ
Earth radius km r_{eq}
Earth-spacecraft distance km r
Eccentricity - e
Hohmann transfer duration s t_H
Inclination ° i
Latitude argument difference between two spacecrafts ° Δu
Orbital velocity km/s V_0
Right Ascension of the Ascending Node ° Ω
Semi major axis km a
True anomaly ° ν
Velocity change km/s ΔV

satellite launch tests conducted by China (2007), India (2019) or even Russia (2021) make this problem particularly tangible. However, regulations on the end-of-life of satellites are almost non-existent, both at the international and national levels. Although France is a pioneer with its law on space operations (LOS), passed in 2008, it has not yet been followed by the other space powers. For now, there are only non-binding recommendations formulated by the European Space Agency (ESA), including the deorbitation of satellite and launcher in less than 25 years (Inter-agency Space Debris Coordination Committee, 2002; Yakovlev, 2005).

These preventive measures will probably not be sufficient to reduce, or event stabilize the amount of debris in LEO. An effective reduction in the number of debris can be achieved through two complementary methodologies. The first solution consists in a circular economy, called "in-orbit servicing IOS", whose principle is to maintain satellites at the end of their life, by recharging them with propellants (refueling), repairing or changing defective parts, to extend their mission time. They then remain active longer and delay the moment when they become debris. Another solution is to perform Active Debris Removal (ADR), and to capture and accelerate the atmospheric reentry of debris. Previous studies show that at least 5 debris per years have to be actively removed to prevent further population increase (Lewis et al., 2012).

One way to reduce the costs of an ADR mission is to remove several pieces of debris per mission, and thus minimize launch costs. However, there are many challenges involved in designing a multi-target debris removal mission. First, the size of the debris population, as well as their orbital parameters, raises a problem of optimizing the choice of debris to remove. Then, the optimization of the trajectory between the different selected debris corresponds to an optimization problem similar to the Traveling Salesman Problem (TSP). TSP is an optimization problem in which the shortest path to visit a given set of cities must be found. This problem may seem simple, but there is no algorithm to solve this problem in a Nondeterministic Polynomial time (NP-complete combinatorial problem). In our case study, each city corresponds to a space debris that must be encountered on its orbit. Thus, the debris to be visited must be selected and ordered in such a way as to minimize the propellant consumption of the spacecraft or at least to keep it low enough to be achievable, while minimizing the mission duration to perform several debris removals in a reasonable amount of time, which corresponds to solving a multi-objective problem (Barbee et al., 2011). In a perfect Keplerian system, only the ΔV

boost is needed to move from one debris to another. However, the gravitational fluctuations related to the flattening of the Earth's poles generate a drift of the debris' orbits, making some orbits out of plane with other ones. Taking this drift into account represents a real issue that makes this trajectory optimization problem particularly complex.

Numerous studies have already been carried out to solve this TSP-like problem and to develop scenarios for IOS or ADR missions targeting several pieces of debris per mission. Since navigating between several out-of-plane orbits involves out-of-plane maneuvers, which are very costly in ΔV, these studies focus to favourable cases. Thus, the number of pieces of debris per mission is generally set at around 5, to correspond to international recommendations. Moreover, the initial list of targets is usually filtered to have the most coplanar orbits possible, and reduce the overall ΔV cost of a mission. So, in (Zuiani and Vasile, 2012), the 5 debris of the ADR mission are previously set with similar inclinations; in (Carlo et al., 2017 and Braun et al., 2013), 5 debris are picked up in a list of respectively 25 and 15 debris filtered such as the inclination is almost the same; and in (Cerf, 2013; Cerf, 2015), 5 debris in Sun-Synchronous Orbits (SSO) are selected among a list of respectively 11 and 25 targets whose inclination is regularly ranged with a small maximum deviation (less than 2°).

The objective of this paper is to plan the architecture of a multi-target ADR mission with an optimized trajectory, but this time without imposing any initial criteria on the orbital parameters. The objective is to optimize the trajectory regardless of the initial debris list, so that it is designed according to the needs and criteria chosen by the user (largest debris, most likely to collide, geostationary debris to be serviced, etc). The challenge of dealing with several pieces of debris in one mission, minimising both ΔV and time costs, is then more difficult to achieve, since the orbits are very likely to be totally non-coplanar, with large deviations in inclination for example, making costly out-of-plane maneuvers necessary.

Thus, we develop a code to determine the trajectory between several orbiting targets, optimising the classification of the set of targets to determine the number of missions required, as well as the order of passage of the debris per mission. This code must be sufficiently robust and generic to be applied and adapted according to the case. Section 2 presents the general framework of the study, outlining the orbital mechanics employed, as well as the possible scenarios for an ADR mission. Section 3 defines the strategies applied to achieve a transfer between targets, as well as the associated equations to calculate the time and ΔV consumption of a mission. Section 4 presents the problem of trajectory optimization and the existing methods for solving it. Section 5 describes the methodology used in our study to solve the trajectory optimization problem, with a presentation of the applied algorithm. At last, Section 6 presents the results obtained on an application case of 50 pieces of debris, identified as the most dangerous by (McKnight et al., 2021). These results are then discussed, followed by the conclusion and perspectives.

2. General framework of the ADR mission

Since the cost of deorbit missions is a major factor for their feasibility, they will have to be multi-targeted in order to deorbit several debris in one mission, which requires determining an optimized trajectory between the targets. Indeed, the debris to be processed with the same mission are spread over different orbits, it is a multi target mission whose propellant cost must be minimized. This implies:

- Associate with each spacecraft a list of debris to be deorbited, thus constituting optimal groups of debris.
- Optimize, for each mission, the maneuvers to be performed to pass from one debris to another in order to minimize the quantity of propellant used.

First, this section reviews the notions of orbital mechanics that are the basis of any trajectory calculation (2.1), as well as the different possible debris removal scenarios (2.2). The general assumptions of the mission architecture are then presented (2.3).

2.1. Orbital mechanics

The motion of a satellite can be defined in the Cartesian reference frame by three positions and three velocities $(x, y, z, \dot{x}, \dot{y}, \dot{z})$. This reference frame is not practical to interpret physically over time. An alternative formalism is used, the Keplerian reference frame, with six orbital parameters describing the shape of the orbit with the eccentricity e and the semi-major axis a, the position of the plane of the orbit with the inclination i and the Right Ascension of the Ascending Node (RAAN) Ω, the position of the orbit in the plane with the Argument of Perigee ω, and the position of the satellite in the orbit with the True Anomaly v. These six orbital parameters $(a, e, i, \Omega, \omega, v)$ are illustrated in Fig. 1. In the case of a circular orbit, $e = 0$ and $\omega = 0$, the important remaining orbital parameters are (a, i, Ω, v).

The orbit parameters can vary in time around their mean, or nominal, value due to external perturbations. Thus, for the case of low orbits, with an altitude of less than 600 km, atmospheric residues generate a drag that affects the eccentricity and the semi-major axis. In geostationary orbit, the solar radiative pressure affects the eccentricity. Finally, the flattening of the Earth induces perturbations of the Earth's gravitational potential, represented by zonal harmonics whose predominant term is J_2. This term generates a drift of the orbit plane by influencing the Ω parameter. It is this last point that imposes a time dependency on the trajectory optimization problem, and is therefore an important issue to take into account.

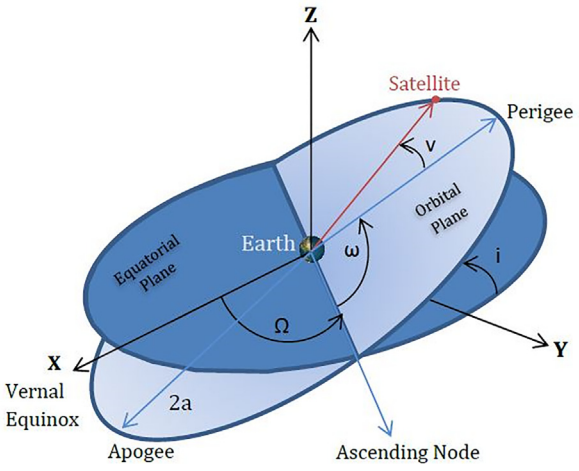

Fig. 1. Scheme of the six orbital parameters in a Keplerian reference frame.

2.2. Mission strategies

Numerous studies have been conducted in recent year to built the architecture of IOS or ADR missions. They are based on two distinct types of technologies: contact and contactless technologies. Contact technologies consist in deploying a system that physically captures the debris, whether it is a harpoon (Dudziak et al., 2015; Sizov and Aslanov, 2021), a robotic arm, or a net (Botta et al., 2019; Lavagna et al., 2012; Cercos et al., 2014). The risk is to miss the capture of the debris during the maneuver, and to generate other micro-debris if the capture is not successful, especially in the case of harpooning. Contactless technologies, on the other hand, rely on the emission of a laser beam or an ion beam (Bombardelli and Pelaez, 2011; Kitamura et al., 2011) to push the debris towards an atmospheric re-entry orbit, and thus free themselves from the problem of contact performance. However, these technologies require a high precision in Guidance-Navigation-Control (GNC) of the servicer (Colmenarejo et al., 2012), to achieve an optimal beam, and can only be applied to debris of modest size: it would require a considerable force to push a debris of several tons to an atmospheric re-entry orbit. In both cases, few real-life tests have been conducted, due to the technical difficulties and the cost that such an operation would represent (Wiedemann et al., 2013).

The most notable demonstration mission is RemoveDEBRIS (Aglietti et al., 2020), an experimental minisatellite sent in 2018 by ESA to test in-flight harpoon and net technologies in a scaled-down format, applied to fictitious debris. The performance of the capture systems was in agreement with the tests carried out on the ground, allowing their Technical Readiness Level (TRL) to be increased. Subsequently, as part of its "zero debris" strategy for 2050, ESA launched a programme called ADRIOS ("Active Debris Removal/ In-Orbit Servicing") to conduct a clean-up of its non-operational and therefore useless satellites and satellite debris in low Earth orbit. A call for tenders has therefore been issued by ESA to finance several demonstration missions to be sent between 2025 and 2030 to validate in-flight technologies for in-orbit services such as refuelling, maintenance or debris removal. The companies involved include Thales Alenia Space and Astroscale, demonstrating the growing interest and involvement of industry in this new market.

In the case of a physical capture of the several targeted debris, many scenarios can be considered (Braun et al., 2013; Cerf, 2013). Either the servicer deploys a deorbiting kit which is added to the debris, this kit then ensures the accelerated deorbiting of the debris by deploying a passive deorbiting system, such as a drag sail (Black and Spencer, 2020; Colombo et al., 2017) or an electrodynamic cable (Barbee et al., 2011), or by integrating a propulsive system leading to a controlled re-entry of the debris (Nowakowski et al., 2019). The servicer satellite leaves the targeted debris once the kit is jettisoned to travel to the next piece of debris.

Another possibility consists in taking the debris on an atmospheric re-entry orbit directly with the help of the servicer satellite, which remains attached to the debris to release it at low altitude (h = 400 km). The servicer then returns to the next piece of debris. This second option allows the servicer not to have to carry kits, at the cost of a larger mass of propellant to effectively perform the up-and-down maneuvers.

These maneuvers can be carried out with a chemical or electric propulsion. In the case of chemical propulsion, with high thrust power, the time of the maneuvers is considered negligible compared to the duration of the transfers between two debris, and the impulse regime model can be applied. In the case of an electric propulsion, with low thrust power, the maneuver time is no longer negligible, and the models imply a continuous thrust. The servicer then performs spiral transfers, to lower the perigee of the debris and to travel between each piece of debris (Zuiani and Vasile, 2012; Carlo et al., 2017).

2.3. Assumptions of the mission

Through related works, Capgemini Engineering has chosen to develop a deorbit kit spacecraft concept to be attached on LEO debris to increase its drag and accelerate its atmospheric re-entry. Once a kit is mounted on the debris, the servicer spacecraft disconnects the kit and the drag augmentation device is deployed, accelerating the deorbitation of the debris, while the spacecraft remains on the initial orbit of the debris.

The removal operation is complex and needs to satisfy operational constraints and performance specifications. Contact capture technologies are more mature than contactless technologies, so we consider the case of physical capture of debris, with a deorbiting kit to then deorbit the debris autonomously. Thus, the trajectory of the servicer is only made of transfer phases to go from one debris

to another, and operation phases near the debris to carry out the capture and kit release operations. The technology used to de-orbit the debris is outside the scope of this study, as well as the maneuvers for approaching the debris in the context of an Orbital Rendezvous operation. This choice of mission architecture enables the trajectory algorithm to adapt to the case of on-orbit servicing, where the scenario is similar. We thus develop a very generic model, whose initial parameters must be not very constraining, while remaining very robust whatever the application use case. The key hypotheses and constraints associated with a deorbit kit delivery spacecraft are summarized below:

- The carrier spacecraft is injected by the launcher into the same orbit and in the same position as the first piece of debris, so that no maneuver is required to reach the target.
- During the removal operation, the kit-carrier spacecraft and the debris have the same states (velocity, position) at the same time, assuming that the effect of J_2 will affect both their orbits in the same way.
- As the majority of satellites and debris have circular orbits, only this case is considered.
- The relative attitude between the debris and the chaser is not taken into account for our study, because the ΔV budget for attitude control is negligible compared to the ΔV budget for orbit change maneuvers.
- A parking time of 7 days is considered in the mission time to provide close proximity and removal operations.

In addition, the spacecraft propulsion is assumed to be chemical, thus the spacecraft maneuvers are instantaneous and follow Tsiolkovski's equation. The maneuvers are therefore either in-plane to modify the semi-major axis by applying the Hohmann transfer, or out-of-plane to correct the inclination and the RAAN.

Between two maneuvers, spacecraft dynamics is described by the following set of Ordinary Differential Equations (ODEs):

$$\begin{cases} \ddot{x} = -\frac{\mu_x}{r^3}\left(1+\frac{3}{2}J_2\left(\frac{r_{eq}}{r}\right)^2\left(1-5\left(\frac{z}{r}\right)^2\right)\right) \\ \ddot{y} = -\frac{\mu_y}{r^3}\left(1+\frac{3}{2}J_2\left(\frac{r_{eq}}{r}\right)^2\left(1-5\left(\frac{z}{r}\right)^2\right)\right) \\ \ddot{z} = -\frac{\mu_z}{r^3}\left(1+\frac{3}{2}J_2\left(\frac{r_{eq}}{r}\right)^2\left(3-5\left(\frac{z}{r}\right)^2\right)\right) \end{cases} \quad (1)$$

which describes the Keplerian motion perturbed by an oblate Earth J_2 term, of Earth Gravitationnal Constant μ, radius r_{eq}, and with r the distance Earth-spacecraft. However, when the spacecraft operates a debris removal operation, its state is considered identical to the one of the debris.

The number of targets per mission is not imposed, in order to optimize the debris groupings per mission according to the orbital parameters. Thus, the problem is optimized by weighting the mission duration and the maximum tolerated propellant consumption, and maximum thresholds must be defined. In order to remain in the common order of magnitude of orbital transfers, we assume to use a maximum ΔV of 4 km/s for each removal mission. Also, assuming that multiple ADR missions can be launched in parallel, mission duration up to 3 years are accepted.

3. Body-to-body transfers

From a list of targeted debris, we aim to form N groups of n debris, where each group is optimized such that:

- The total ΔV of a mission (associated with the maneuvers required to move from one piece of debris to the other) is minimal
- The time Δt of the mission is minimal.

Therefore, an orbit changing approach need to be implemented: $(a_1, e_1, i_1, \Omega_1, \omega_1, v_1) \rightarrow (a_2, e_2, i_2, \Omega_2, \omega_2, v_2)$.

Since the debris are assumed to have quasi-circular orbits, the maneuvers on the eccentricity e and the perigee argument ω can be neglected. This leaves us to deal with the remaining 4 orbital parameters: (a, i, Ω, v). The proposed strategy is to make a maneuver for the inclination, then a Hohmann transfer type maneuver which would allow one to change the semi-major axis in one hand, and to make the orbital rendezvous in other hand.

Regarding the longitude of the ascending node Ω, several scenarios are envisaged:

- **Scenario 1**: Use the natural drift in Ω due to the flattening of the Earth (J_2 term) inducing a drift time Δt.
- **Scenario 2**: Perform a maneuver in Ω.
- **Scenario 3**: Perform hybrid missions using the J_2's drift but also Ω maneuvers.

Since out-of-plane maneuvers are the most expensive, scenario 2 will have a total ΔV much higher, typically 2–9 km/s higher per mission. Scenario 1, on the other hand, will result in increased mission duration, as the phasing time between the Ω parameters may be very long. Thus, in his study, (Cerf, 2013) proved that this phasing time required depends on the range $\Delta\Omega$ and the range between their drifts $\Delta\dot{\Omega}$ such that:

$$t = -\frac{\Delta\Omega}{\Delta\dot{\Omega}} \quad (2)$$

Eq. (2) implies considerable phasing duration in the case where the orbits are similar, which induces a very small $\Delta\dot{\Omega}$ term, and in the case where the debris and the spacecraft are misplaced, so that the drift of their parameter increases the $\Delta\Omega$ range. This last case is illustrated in Fig. 2. In the worst case, the natural alignment of the Ω parameters can take up to several months.

In order to make a compromise between a not too high ΔV and a reasonable drift time, scenario 3 proposes a com-

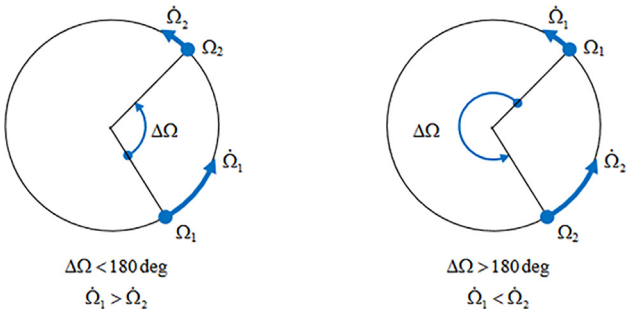

Fig. 2. Forward or backward correction on the Ω parameter (Cerf, 2013).

bination of the two first scenarios that will permit to play on the time and propellant constraints imposed by the future missions.

Thus, to summarise, the spacecraft achieves its transfer from one piece of debris to another in three steps::

1. Drift or maneuver to align the Ω parameter
2. Change of the inclination
3. Phasing between the two objects to end up at the same spot in the orbit

The equations needed to perform the impulse maneuvers, both in-plane and out-of-plane, are presented in Section 3.1, while the equations calculating the drift time needed to naturally align the Ω parameters are presented in Section 3.2. Lastly, Section 3.3 explains the implementation of the phasing phase. The propagation of the trajectories is achieved by solving the equations presented below in Python.

3.1. Equations of ΔV for maneuvers

For in-plane maneuvers (Δa), a classical Hohmann transfer is used as debris are assumed to have near-zero eccentricity. Eq. (3) and Eq. (4) describe the cost for the modification of the semi-major axis from a circular orbit (O_1) with radius r_1 to another one (O_2) with radius r_2 using Hohmann transfer, while the Fig. 3 shows a scheme of all the maneuvers.

The latter consists in the succession of 2 increments of velocities ΔV_1 and ΔV_2 to leave an initial orbit O_1 and reach the orbit of the target debris O_2 with the same position and velocity. The velocity increment ΔV_1 must be performed in the direction of the velocity vector to place the spacecraft in an elliptical transfer orbit that will take it toward the second orbit. Then, when the spacecraft reaches the apogee of the transfer orbit, the application of a burn ΔV_2 in the direction of the velocity vector is applied. The time required to complete an entire Hohmann transfer is defined by Eq. 5.

$$\Delta V_1 = \sqrt{\frac{\mu}{r_1}}\left(\sqrt{\frac{2r_2}{r_1+r_2}} - 1\right) \tag{3}$$

$$\Delta V_2 = \sqrt{\frac{\mu}{r_2}}\left(\sqrt{\frac{2r_1}{r_1+r_2}} - 1\right) \tag{4}$$

$$t_H = \pi\sqrt{\frac{(r_i + r_f)^3}{8\mu}} \tag{5}$$

The analytical method used to calculate out of plane maneuvers ($\Delta i, \Delta\Omega$) are based on Gauss's variational equations for circular orbits (Gauss, 1864), where V_0 is the velocity of the spacecraft at the moment of the maneuver. These maneuvers are performed by doing an impulse perpendicular to the orbital plane, where the initial and final orbits intersect.

Eq. (6) describes the modification of the orbit inclination, presented on Fig. 4. This maneuver is preferentially done at the ascending or descending node, perpendicular to the orbital plane. Inclination maneuvers are very expensive, but remain necessary since J_2 does not modify the inclination.

Eq. (7) describes the cost for the adjustement of the RAAN difference. This maneuver is performed at the intersection of the two orbits, as shown on Fig. 5. As this out-of-plane maneuver is extremely costly, we will take maximum advantage of the natural drift of the RAAN to adjust the orbits, according to the time constraints of the missions.

$$\Delta V_i = 2V_0 \sin\left(\frac{\Delta i}{2}\right) \tag{6}$$

$$\Delta V_\Omega = 2V_0 \sin\left(\frac{\Delta\Omega}{2}\right) \tag{7}$$

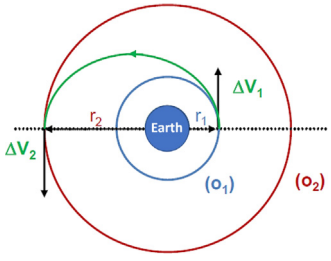

Fig. 3. Hohmann transfer.

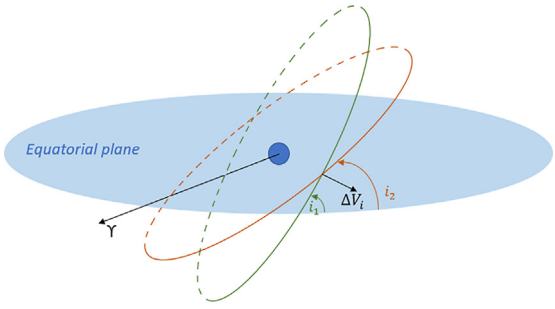

Fig. 4. Inclination maneuver.

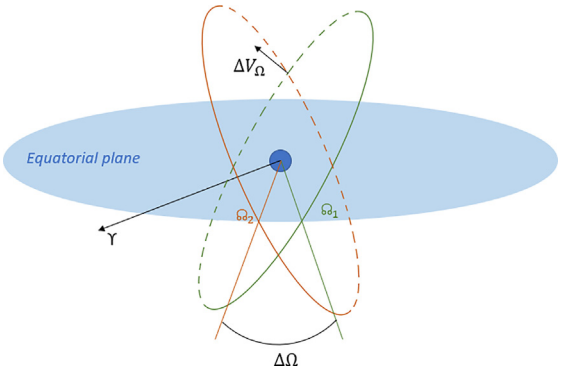

Fig. 5. RAAN maneuver.

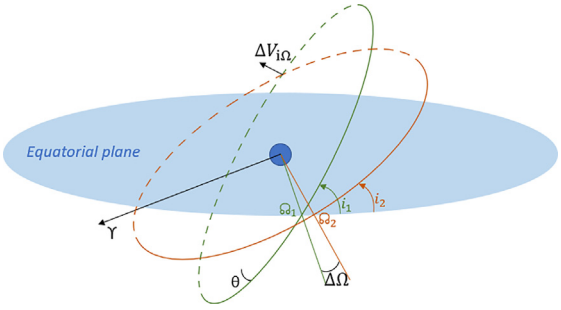

Fig. 6. Inclination and RAAN combined maneuver.

However, it is possible to combine maneuvers in i and Ω in order to reduce the ΔV needed. The thrust must be done at the intersection of the planes of the spacecraft and the debris to reach, as illustrated on Fig. 6. The ΔV needed is given by Eq. (8). The angle θ between the two orbits, including both a change in angle i and a change in angle Ω, is defined by Eq. (9), with i_1 and i_2 the inclination of the spacecraft before maneuver and the inclination of the debris to reach, respectively.

$$\Delta V_{i\Omega} = 2V_0 \sin\left(\frac{\theta}{2}\right) \tag{8}$$

$$\theta = \arccos(\cos(\Delta\Omega)\sin(i_1)\sin(i_2) + \cos(i_1)\cos(i_2)) \tag{9}$$

3.2. Equations of Δt drift for Ω

The drift of Ω is induced by the flattening of the Earth represented by zonal harmonics whose predominant term is J_2. In the framework of the quasi-circular approximation (for eccentricity $e \approx 0$), the Gaussian equation describing the drift is written:

$$\frac{d\Omega}{dt} = -\frac{3}{2} n \left(\frac{r_{eq}}{a}\right)^2 J_2 \cos(i) \tag{10}$$

where $n = \sqrt{\frac{\mu}{a^3}}$ is the mean motion of the debris, i.e. the mean angular speed during a period, in $rad.s^{-1}$.

Eq. (10) involves two orbital parameters: the semi major axis a and the inclination i. These two parameters are considered constant during the drift, it allows us to write the evolution of Ω over time according to the initial Ω_0:

$$\Omega(t) = -\frac{3}{2} n \left(\frac{r_{eq}}{a}\right)^2 J_2 \cos(i)t + \Omega_0 \tag{11}$$

As a consequence, for two debris k and l, we have:

$$\Omega_k(t) = -\frac{3}{2} n_k \left(\frac{r_{eq}}{a}\right)^2 J_2 \cos(i_k)t + (\Omega_k)_0 \tag{12}$$

$$\Omega_l(t) = -\frac{3}{2} n_l \left(\frac{r_{eq}}{a}\right)^2 J_2 \cos(i_l)t + (\Omega_l)_0 \tag{13}$$

$$\Omega_k(\Delta t) \equiv \Omega_l(\Delta t) \pmod{2\pi} \tag{14}$$

where Δt represents the drift time required to equalize the longitudes of the ascending node between the two debris.

By doing (12)–(13) and isolating t, we find the solution of this system which is:

$$\Delta t_{(k,l)} = -\frac{2}{3} \frac{(\Omega_k)_0 - (\Omega_l)_0}{J_2 r_{eq}^2 \left(\frac{n_l \cos(i_l)}{a_l^2} - \frac{n_k \cos(i_k)}{a_k^2}\right)} \tag{15}$$

For example, we take the case of a group consisting of 5 pieces of debris, which requires 4 transfer phases, such as $G = d_0, d_1, d_2, d_3$. The time intervals Δt between two debris are dynamically calculated as follows:

1. We instantiate a dynamic matrix Ω initialized with the values of the RAAN parameters issued from the data-frame associated with the debris $(d)_{i=0,..,3}$, such as:

$$\mathbf{\Omega} = \begin{pmatrix} (\Omega_0)_{t_0} & 0 & 0 & 0 \\ (\Omega_1)_{t_0} & 0 & 0 & 0 \\ (\Omega_2)_{t_0} & 0 & 0 & 0 \\ (\Omega_3)_{t_0} & 0 & 0 & 0 \end{pmatrix} \tag{16}$$

2. We calculate Δt_1 between $(\Omega_0)_{t_0}$ and $(\Omega_1)_{t_0}$ according to Eq. (15).
3. We propagate the $(\Omega_i)_{t_0}$ for $i = 1, 2, 3$ during Δt_1 and update the matrix:

$$\mathbf{\Omega} = \begin{pmatrix} (\Omega_0)_{t_0} & 0 & 0 & 0 \\ (\Omega_1)_{t_0} & (\Omega_1)_{t_0+\Delta t_1} & 0 & 0 \\ (\Omega_2)_{t_0} & (\Omega_2)_{t_0+\Delta t_1} & 0 & 0 \\ (\Omega_3)_{t_0} & (\Omega_3)_{t_0+\Delta t_1} & 0 & 0 \end{pmatrix} \tag{17}$$

4. We calculate Δt_2 between $(\Omega_1)_{t_0+\Delta t_1}$ and $(\Omega_2)_{t_0+\Delta t_1}$.
5. We propagate the $(\Omega_i)_{t_0+\Delta t_1}$ for $i = 2, 3$ during Δt_2 and update the matrix:

$$\mathbf{\Omega} = \begin{pmatrix} (\Omega_0)_{t_0} & 0 & 0 & 0 \\ (\Omega_1)_{t_0} & (\Omega_1)_{t_0+\Delta t_1} & 0 & 0 \\ (\Omega_2)_{t_0} & (\Omega_2)_{t_0+\Delta t_1} & (\Omega_2)_{t_0+\Delta t_1+\Delta t_2} & 0 \\ (\Omega_3)_{t_0} & (\Omega_3)_{t_0+\Delta t_1} & (\Omega_3)_{t_0+\Delta t_1+\Delta t_2} & 0 \end{pmatrix} \tag{18}$$

6. We calculate Δt_3 between $(\Omega_2)_{t_0+\Delta t_1+\Delta t_2}$ and $(\Omega_3)_{t_0+\Delta t_1+\Delta t_2}$.

The matrix $\mathbf{\Omega}$ may vary in size depending on the number of pieces of debris in a group.

3.3. Phasing phase

For the phasing maneuver and final rendezvous, several methods have been considered such as the use of Lambert arcs or the optimization of trajectory via optimal control methods. These methods proved to be either not optimal enough (ΔV too important) or too complex (considering the early phase of the work). It is finally the Hohmann transfer which appeared to be the best compromise between fidelity and complexity.

Thereby, some approximations are assumed. First, we suppose that before the phasing maneuver, the spacecraft and the piece of debris (i.e. the target) are in circular and coplanar orbits, which is validated by the two previous maneuvers, and by the fact that the eccentricity of the debris is assumed to be null. Secondly, the spacecraft and the target are only subject to the gravitational attraction of the Earth during this maneuver. This is justified by the fact that the duration of a Hohmann transfer is of the order of an hour (Eq. (5)). The drift of the orbital parameters due to the gravitational perturbations on such a short duration is not significant and the approximation has a very limited impact on the fidelity of the model.

The parameter to be determined now is the instant at which the spacecraft must perform its first Hohmann maneuver ΔV_1 (Eq. (3)) to join the orbit of the target. To do so, the velocity increment should be applied when the difference Δu between the latitude argument of the spacecraft and the latitude argument of the target debris is:

$$\Delta u = \pi\left(1 - \sqrt{\frac{r_i + r_f}{2r_f}}\right) \tag{19}$$

The latitude argument of a satellite being defined as: $u = v + \omega$ where v is the true anomaly and ω is the argument of the perigee.

Thus, we propagate the trajectory until the spacecraft meets the target, i.e., after having let itself drift on its transfer orbit during a half-period. Then the second maneuver of the Hohmann transfer is performed, with the application of a ΔV_2 (Eq. (4)) in the direction of the velocity vector of the spacecraft.

Once this sequence of maneuvers is completed, the spacecraft performs its orbital rendezvous to join the target. The rendezvous and docking phase is not addressed in this work. We assume that the ΔV and time for this phase is not significant in regard of the overall mission.

4. Formulation of the trajectory optimization problem

Orbital mechanics, time and maneuver equations, and the overall sequencing of a multi-target mission have been defined. It now remains to determine the classification of the targets into several ADR missions, as well as the order of passage between targets within a mission, in order to minimize propellant and drift time costs.

The problem of optimising the trajectory between several targets corresponds to a "Travelling Salesman Problem", which is presented and related to our study in 4.1, while 4.2 reviews the existing solutions to this type of problem, as well as the application cases already studied in the literature.

4.1. Trajectory optimization

The classification of debris for removal operation is intended to produce subsets of the overall debris population under consideration. An optimal path between each debris must be found to minimize the total ΔV required. This induces to remove as much debris as possible per mission, which helps to minimize mission costs, reduce the timeframe required to complete a debris removal mission, and maximize the payload mass available on the removal spacecraft for a given debris removal system (Barbee et al., 2011;(Braun et al., 2013)).

In other words, the development of the mission architecture aims at solving a trajectory optimization problem such as the TSP, where each piece of debris of the considered list must be visited once, while minimizing the travel time and cost (Izzo et al., 2015; Cerf, 2013). However, the ADR optimization problem is much more complex than a classical TSP. On one side, the distance to be optimized is not limited to a single itinerary, but is the sum of multiple ADR missions, each with its own constraints in terms of ΔV, time, and number of kits to be carried. On the other side, the debris evolve at different precession rates, which makes the distances between each pair of debris to vary multi-periodically. Accordingly, the ADR optimization problem is time-dependant (Federici et al., 2019).

This problem was the subject of the Global Trajectory optimization Competition GTOC9, also called "Kessler Run", and developed by ESA. During this one-month competition, it has been imagined that in the year 2060, a serious explosion triggered the Kessler effect, compromising the SSO environment. A set of 123 fictitious orbiting debris pieces has been isolated and, if they are removed, space activities could restart. Multiple missions have to be designed to cumulatively remove all the debris pieces. Each mission cost depended on the spacecraft mass and a base increasing cost. The design of the Challenge and the methodologies and results obtained by the participating teams are related in (Izzo and Luís, 2018).

4.2. Metaheuristic solutions

This optimization problem is an NP-complete combinatorial optimization problem, since the number of permutations of the target spacecraft order is practically impossible to sample exhaustively for an interesting number of debris. Therefore, it is impossible to solve the problem by exact calculation, it is necessary to use approximate solutions,

or heuristics, to determine a solution close to the optimal or exact solution within an accessible calculation time. Over the years, several heuristics have been developed, some of them working incrementally by building a solution in the form of a decision tree; other heuristics working on a single chain (Chmait and Challita, 2013). A list of heuristics, presented in the context of another combinatorial optimization problem, the Vehicle Routing Problem (VRP), is shown in Fig. 7.

The most popular one correspond to variants of the genetic algorithm GA, simulated annealing SA, tabu search, and the ant colonisation algorithm ACO (Chmait and Challita, 2013). These heuristics have been adapted to the case of a time-dependent TSP-like problem such as ADR or IOS missions. Thus, (Bourjolly et al., 2006) uses exact computation and the Tabu algorithm to determine the best trajectory between 10 out-of-service satellites to be repaired as part of in-orbit servicing, using chemical propulsion. (Cerf, 2013) applies the branch-and-pound method to simultaneously optimize the grouping of 5 of 11 pieces of debris and the orbital maneuvers to be performed, using chemical propulsion. (Carlo et al., 2017) applied the physarium algorithm, similar to the ACO algorithm, to optimize the number of pieces of debris to be deorbited per mission, as well as the sequence of maneuvers to be carried out, in the case of LEO satellites, using electric propulsion. In the case of the GTOC9 challenge, many teams applied a mix of ACO and branch-and-pound heuristics (Izzo and Luís, 2018). (Kanazaki et al., 2018) applied the genetic algorithm to a set of 100 pieces of debris to be deorbited. Last, (Han et al., 2019; Federici et al., 2019; Cerf, 2015) used simulated annealing to respectively build the architecture of IOS missions on GEO satellites and ADR missions on LEO and SSO satellites.

Among these functions, simulated annealing is particularly designed to solve difficult combinatorial optimization problems and is therefore very well suited to the development of ADR mission architecture. This method has the advantage of being easy to implement and understand, as it is based on solid theoretical principles derived from a real mechanical phenomenon. Moreover, simulated annealing does not need to be parameterized with many initial constraints, which makes it very robust and flexible, applicable on different study cases. It can deal with non-linear problems, which is the case of time-dependent ADR missions and is able to avoid local minima. In theory, the algorithm can converge to the real optimal solution of the problem, at the cost of a very small iteration step and thus an infinite computation time. In practice, it is not guaranteed that the optimal solution determined by the algorithm corresponds to the true optimal solution of the problem. However, the determined solution is often close to the optimal solution. The main disadvantage of the method lies in the compromise between the refinement of the step size and

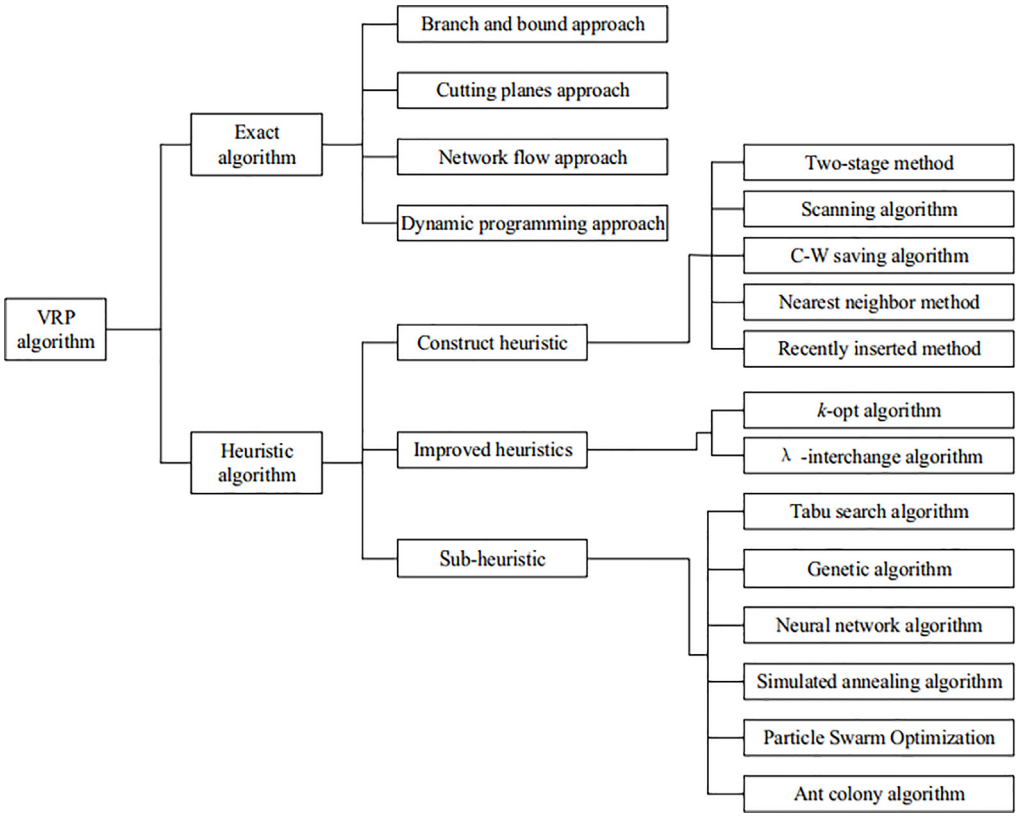

Fig. 7. Classification of heuristics (Zhang et al., 2022).

the computation time tolerated. This disadvantage can be overcome by parallelizing the code, which is possible in the case of simulated annealing (Busetti, 2001; Federici et al., 2019).

5. Resolution of the optimization problem

Simulated annealing originates from metallurgy, where the strengthening of a metal is achieved by successively cooling and heating the metal until it achieves the desired mechanical properties. Thus, in the case of solving a TSP problem, an initial state is generated, often randomly. In the classical TSP case, this corresponds to a trajectory between the set of cities to be visited. A fictitious temperature T is applied to the material, and is progressively lowered to a final temperature. At each temperature, for a certain number of cycles, corresponding to iterations, the initial state is modified by swapping cities, for example. If the new situation corresponds to a better solution, then this new state is kept. On the contrary, if the new situation is worse, it is only kept if a probability law is validated. This law avoids being locked into local minima, and allows the process to cover all possible states even if some states correspond to very poor performance. The process stops when the temperature reaches a set final temperature (Kirkpatrick et al., 1983). This gradual cooling process, the rate of which can be adjusted by the user, is the strength of the simulated annealing. The slower the rate, the more the algorithm scans the set of possible solutions and converges on the optimal solution. This enables it to solve large problems with many local optima.

5.1. State and neighbourhood

In our study, we start with a predefined list of debris to be removed, according to the use case considered. All the debris on this list is randomly divided into different groups, with no criteria for the number of debris per group. Each group constitutes an ADR mission and this corresponds to the initial state. The objective is to calculate the ΔV and the time required to complete each mission, then to modify the groups and distribute the debris in such a way that each mission requires a $\Delta V_{max} \leqslant 4$ km/s and less than 3 years of mission time. The distribution of the N_{debris} debris considered in N_{group} missions corresponds to the state X of the system, and is described as followed:

$$X \in M_{N_{debris},N_{group}}(\{0,1\}) \tag{20}$$

where $X_{i,j} = 1$ if the debris i is in group j and 0 otherwise. Thus, on the example of a statement detailing 5 pieces of debris divided into 3 groups, we obtain a matrix X with 5 rows and 3 columns in the followed form:

$$X = \begin{array}{c} \\ Debris\ 1 \\ Debris\ 2 \\ Debris\ 3 \\ Debris\ 4 \\ Debris\ 5 \end{array} \begin{array}{c} \begin{array}{ccc} Group\ 1 & Group\ 2 & Group\ 3 \end{array} \\ \begin{pmatrix} 1 & 0 & 0 \\ 1 & 0 & 0 \\ 0 & 1 & 0 \\ 0 & 1 & 0 \\ 0 & 0 & 1 \end{pmatrix} \end{array} \tag{21}$$

The length of the matrix is therefore defined by the total number of debris N_{debris} considered, and a priori set on a use case. The width depends on the number of missions N_{group} in which this debris is distributed, and may vary from one iteration to another.

The distribution of debris in different ADR groups must check the following conditions:

$$\forall k \in [1, N_{debris}], \sum_{l=1}^{N_{group}} X_{k,l} = 1 \tag{22}$$

$$\forall l \in [1, N_{group}], \sum_{k=1}^{n_{debris} \in group_l} \Delta V(X_{k-1,l} \longrightarrow X_{k,l}) \leqslant \Delta V_{max} \tag{23}$$

$$\forall l \in [1, N_{group}], \sum_{k=1}^{n_{debris} \in group_l} \Delta t(X_{k-1,l} \longrightarrow X_{k,l}) \leqslant \Delta t_{max} \tag{24}$$

Eq. (22) means that a debris is affected to one group and only one, while Eq. (23) and (24) mean respectively that the total velocity change and the duration of the mission have to be lower than ΔV_{max} and Δt_{max}, two values set by the user.

Thus the state X is a matrix in which the lines represent every debris, and the columns the groups in which they are. This state does not take into account the order of the debris the spacecraft has to follow to minimize the ΔV and Δt costs.

The neighbourhood corresponds, for a given mission, to the debris distributed in the other missions. We will take for the examples a total of 5 considered debris initially spread in 3 groups. The following matrices represent the state X: the lines represent every debris, and the columns the groups in which they are. Then, a neighbor can be defined in 3 different ways:

1. For a given state X, we select 2 debris in 2 different groups, then we switch them:

$$X = \begin{pmatrix} 1 & 0 & 0 \\ 1 & 0 & 0 \\ 0 & 1 & 0 \\ 0 & \mathbf{1} & 0 \\ 0 & 0 & \mathbf{1} \end{pmatrix} \Rightarrow X = \begin{pmatrix} 1 & 0 & 0 \\ 1 & 0 & 0 \\ 0 & 1 & 0 \\ 0 & 0 & \mathbf{1} \\ 0 & \mathbf{1} & 0 \end{pmatrix} \tag{25}$$

2. We select a debris in a group, and move it to another group:

$$X = \begin{pmatrix} 1 & 0 & 0 \\ 1 & 0 & 0 \\ 0 & 1 & 0 \\ 0 & \mathbf{1} & 0 \\ 0 & 0 & 1 \end{pmatrix} \Rightarrow X = \begin{pmatrix} 1 & 0 & 0 \\ 1 & 0 & 0 \\ 0 & 1 & 0 \\ 0 & 0 & \mathbf{1} \\ 0 & 0 & 1 \end{pmatrix} \tag{26}$$

3. A group is selected and then redistributed to other groups:

$$X = \begin{pmatrix} \mathbf{1} & 0 & 0 \\ \mathbf{1} & 0 & 0 \\ 0 & 1 & 0 \\ 0 & 1 & 0 \\ 0 & 0 & 1 \end{pmatrix} \Rightarrow X = \begin{pmatrix} 0 & \mathbf{1} & 0 \\ 0 & 1 & \mathbf{1} \\ 0 & 1 & 0 \\ 0 & 1 & 0 \\ 0 & 0 & 1 \end{pmatrix} \tag{27}$$

These scenarios are not equiprobable in the algorithm. The criteria of ΔV_{max} and Δt_{max} must be met, so the more missions have a huge ΔV or Δt, the less possible it will be to add new debris to them. Thus, case 3 where a group is split to fill others with its debris cannot result in a state meeting the ΔV_{max} and Δt_{max} criteria if the groups are already filled with many debris. Some neighbourhoods are computationally time-consuming, without succeeding in finding a solution. To avoid this case, the neighbourhood probabilities have been set to change with the evolution of the annealing simulation.

At initialization, all the probabilities of the possible neighbouring cases are equal. When the average number of debris per group becomes greater than 3.5, the probability of having the third neighbour becomes: $p(3) = \frac{1}{25}$. The other cases are always equal to each other: $p(1) = p(2) = \frac{12}{25}$. Finally, if there is more than 4.5 pieces of debris per group on average, case 3 will no longer occur, unless there is a group with only one piece of debris, which could possibly be placed in another mission. These probabilities have been chosen empirically, in order to obtain good results without wasting computing time.

5.2. Cost function

The new state $\tilde{X}$ of the system, corresponding to the distribution of the 50 pieces of debris into N_{group} missions, must then be evaluated to determine whether it is better or worse than the previous one X, from a ΔV and mission time point of view. The optimization is therefore bi-objective, with a priori opposite objectives. The evaluation of the system is done by applying a scalarisation method, which consists in transforming the multi-objective problem into a parameterised single-objective problem (Miettinen and Mäkelä, 2002; Shirazi et al., 2018). To do this, a cost function to be minimized is constructed and the weighted sum method is used. This cost function corresponds to the energy E(X) in the framework of simulated annealing, and is defined in such a way that the ΔV and time criteria are taken into account by adding a weighting parameter in front of each of the terms to be minimized:

$$E = \sum_{k_{debris}=1}^{Nb_{group}} \Delta V_k + \frac{V_{tol}}{t_{tol}} \sum_{k_{debris}=1}^{Nb_{group}} \Delta t_{drift,k} \tag{28}$$

For the sake of homogeneity and weights corresponding to the term in ΔV and the drift, we introduce two quantities V_{tol} and t_{tol} that control the trade-off between the ΔV cost and the Δt cost. The quantities correspond to the order of magnitude tolerated for a mission in terms of ΔV and drift time, and could be adjusted in function of the mission constraints. This trade-off can be adjusted, depending on the weight we wish to give to the minimization of ΔV or Δt_{drift}. An optimal solution exists for each of the pairs (V_{tol}, t_{tol}), and the set of these optimal solutions form the Pareto front of our problem.

Eq. (28) takes into account the total ΔV_k of a mission, but also the total drift time $\Delta t_{drift,k}$ associated with group k due to J_2 disturbance and defined in Eq. (15). The transfer strategy is set to be first an inclination and a RAAN maneuver in order to put the spacecraft in the same plane that the debris', and then a Hohmann transfer is done to reach it; thus the ΔV is defined for every transfer between two given debris and no optimization is done on it.

The use of this weighted sum method provides an easy overlap with the different mission scenarios presented previously. Thus, Eq. (28) is the general form of the energy of the system for the hybrid scenario 3, while scenarios 1 and 2 correspond to special cases. By setting $V_{tol} = 0$, maximum weight is given to ΔV_{tot}, with no constraints on the mission time (scenario 1). On the other hand, by setting $t_{tol} = 0$, priority is given to a minimal mission duration, no matter the ΔV budget (scenario 2). The associated optimal solutions correspond to the extreme solutions of the Pareto front.

For a given set of debris, the optimal order of the maneuvers is not known a priori. At each iteration, the order of passage from one piece of debris to another within the i^{th} group is determined such that:

- the Ω parameter is decreasing, in order to minimize the drift time needed to align this parameter between two pieces of debris
- the amount of energy below is minimized, in order to reduce the costs in ΔV and in drift time (which is conditioned by the above criterion):

$$E_k = \Delta V_k + \frac{V_{tol}}{t_{tol}} \Delta t_{drift,k} + \sigma\left(\frac{\Delta V}{V_{tol}}, \frac{\Delta t}{t_{tol}}\right) \tag{29}$$

where σ is a standard deviation term added in order to have more homogeneous results between the ΔV budget and mission time. This term implies that the calculated energy is higher when the standard deviation between the quantities $\frac{\Delta V}{V_{tol}}$ and $\frac{\Delta t}{t_{tol}}$ is high. For example, a very low ΔV will be at the cost of a very high drift time, while a very reduced mission time will be at the cost of a high

ΔV, i.e. at the cost of an out-of-plane maneuver, which could have been avoided with another mission configuration. This term therefore favours transfers where the quantities are equivalent, and limits the scattering of extremes from one group to another.

For hybrid scenario 3, we consider at each iteration the interest of performing a maneuver in RAAN rather than letting the satellite drift by the effects of J_2. We use the parameters $V_{tol} = 1$ km/s and $t_{tol} = 1$ year to normalise the ΔV and Δt parameters and thus be able to compare them with each other, by comparing the quantities $\frac{\Delta V}{V_{tol}}$ and $\frac{\Delta t}{t_{tol}}$. Since we impose as an input criterion that $\frac{\Delta V}{V_{tol}} < 4$ while $\frac{\Delta t}{t_{tol}} < 3$, this means that $\frac{\Delta V}{V_{tol}}$ evolves faster than $\frac{\Delta t}{t_{tol}}$. As we still want to favour the drift in time compared to the Ω maneuver, we impose the latter only when it remains less costly than the drift in time, i.e. when the following condition is satisfied for each iteration of E_k:

$$\frac{\Delta V_{\Omega}}{V_{tol}} < \frac{\Delta t_{J_2}}{t_{tol}} \tag{30}$$

The increasing order of E_k is kept in memory by reading from left to right within a group. Therefore, the metaheuristic also optimizes the trajectory to be performed within a group at the same time as this debris group is constituted.

5.3. Algorithm evolution

Let X be a state, $\tilde{X}$ a neighbor of this state, and T a given temperature. We then encounter two situations:

- If $E(\tilde{X}) < E(X)$, then we keep the state $\tilde{X}$ and continue the algorithm
- If $E(\tilde{X}) > E(X)$, then we keep the state $\tilde{X}$ with the probability $p = e^{\frac{-\Delta E}{T}}$

This rule of acceptance of unfavorable states with an exponential is called dynamics of Metropolis, and it is applied at each iteration of the algorithm. This function is a Markov chain, i.e. the new state only depends on the current one and not on the ulterior ones, however, the probability to keep an unfavourable state decrease with the simulated annealing progression.

In practice, we define an initial temperature T_i and a final temperature T_f, as well as a t_{iter} number of iterations of the Metropolis dynamics to perform for each temperature. Once the number of iterations is done, we decrease the temperature with a geometric factor $\alpha < 1$ such that at the end of the chain of iterations for a temperature T_i, we have $T_{i+1} = \alpha T_i$.

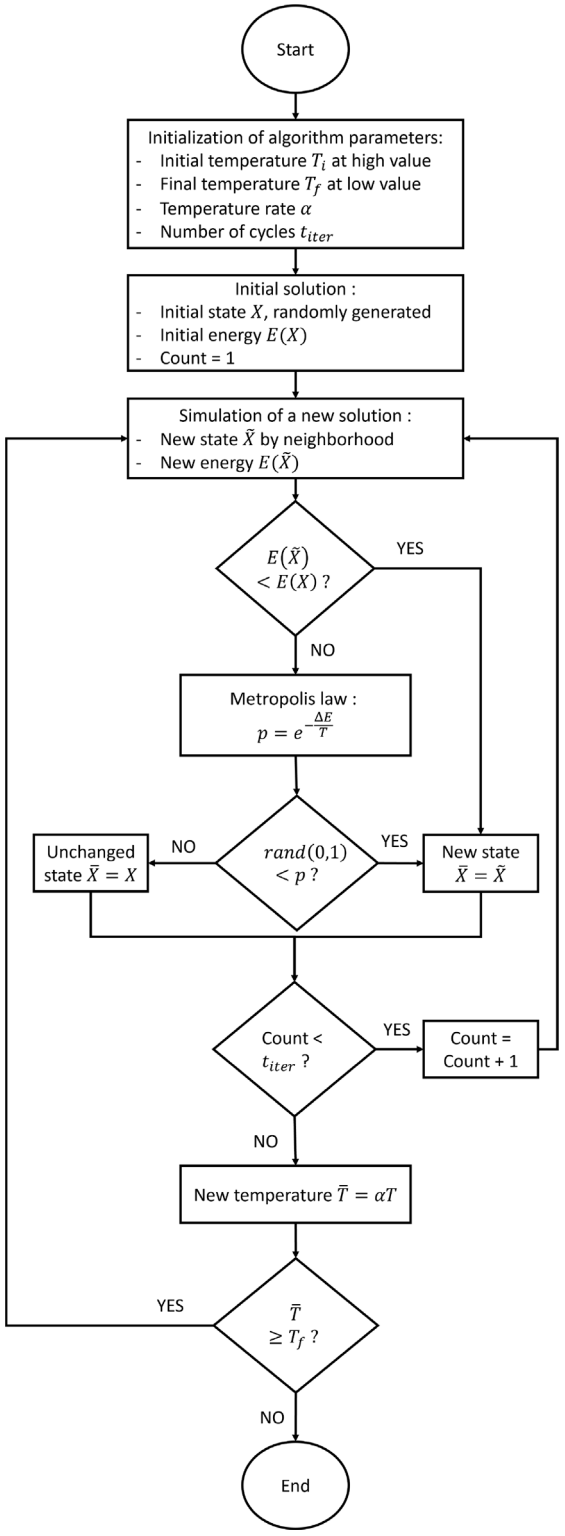

Fig. 8. Workflow of the simulated annealing.

The overall evolution of the code is summarised in a pseudo code presented in Algorithm 1 and illustrated on Fig. 8.

Algorithm 1. Simplified pseudocode of the Simulated Annealing

$T \leftarrow T_i$
while $T > T_f$ **do**:
  $X \leftarrow GenerateRandomState$
  $E \leftarrow energy(X)$
  for i in [1, t_{iter}] **do**
    $\tilde{X} \leftarrow neighbor(X)$
    $\tilde{E} \leftarrow energy(\tilde{X})$
    $X, E \leftarrow Metropolis(\tilde{X}, \tilde{E}, X, E)$
  end for
  $T \leftarrow \alpha T$
end while

6. Application case

This section presents the results obtained by applying our approach to a list of debris to be removed. The debris and their orbital parameters are presented in Section 6.1, and the computational performances associated with our algorithm are indicated in Section 6.2. The time and ΔV matrices to get from one debris to another are presented in Section 6.3. The results in terms of optimized debris groupings are presented in Sections 6.4 and 6.5. Section 6.4 compares the performance in ΔV and Δt obtained according to the scenario considered, imposing for each mission a maximum ΔV and Δt cost. Scenario 1, 2 and 3 are thus compared with the same algorithm and mission parameters. Then, Section 6.5 compares the performance obtained for scenario 3 when the mission is limited in number of debris. Finally, a discussion is held (6.6) on our results and our contribution to the existing literature.

6.1. Targets

The first step is to identify a list of high priority debris targets. To optimize the effectiveness of an ADR mission, the targeted debris must significantly reduce the risk of collisions, referred to as critical debris. To determine them, a list of criteria can be established as follows:

- high mass (they have the greatest impact on their environment in the event of a collision)
- high probability of collision (e.g., in densely populated areas and with a large cross-sectional area)
- high altitude (where the orbital lifetime of the resulting fragments is long and the atmospheric drag is negligeable)

A list of critical debris has been established in the study (McKnight et al., 2021), which concatenates the results of several scientific teams that have each established their own list of the 50 most critical debris in orbit. In this top 50, 39 launchers stages are listed, mostly issued from Zenit and Cosmos USSR Rocket Body during the 90's, against only 11 payloads, including the Envisat (ESA), Adeos (Japan) and Meteor 3 M (Russia) satellites. In terms of mass criteria, two levels stand out:

- Above 4 tons with mainly the SL-16R/B 3rd stage.
- Below the 4-ton class with objects ranging from 1 to 4 tons (28/50 objects).

In terms of targeted orbit, the most densely populated region in LEO is around 800–1000 km altitude at high inclinations, corresponding to the polar SSO orbits. ADR missions must therefore focus on the multi-ton debris located in SSO orbits to maximize the impact of debris removal on improving the space environment.

Therefore, we use this list as a use case for our study, to have a real case where debris removal will have a maximum impact on the improvement of the situation. Such a choice implies that the debris list is not optimized according to the orbital parameters $(a, e, i, \Omega, \omega, v)$, as shown by their distribution, displayed on Fig. 9. Even if most debris have a low enough eccentricity to consider their orbit as quasi-circular, we can observe three quite distinct groups for inclination (71°, 83° and 98°) and about two groups for the semi-major axis (7200 km and 7380 km), which does not correspond to a favorable situation regarding trajectory optimization.

These values are sufficient to have considerable drift rate of the ascending nodes, which should be taking into account. In parallel, a study about the influence of the other perturbations on the debris have been done. The results have shown that the considered debris have too high altitudes so the atmospheric drag does not have an effect on them, and, at the contrary, they are too low so the luni-solar attraction and the solar radiation pressure cannot impact them.

6.2. Computing performance

Table 1 summarises the initial constraints of the problem: our case study has 50 pieces of debris to be divided into a number N_{group} of ADR missions, N_{group} to be defined by the algorithm. For this purpose, the cost in ΔV and Δt of each mission is also reminded. As the orbital parameters vary over time, which affects the optimization of debris consolidation, an initial launch date T_0 is set. The results are therefore given assuming that all ADR missions are launched on this date. In order to plan a mission for 1 year from now, for example, it would be necessary to propagate the orbital parameters of the debris during this period and then give these values as input to the algorithm.

The parameters of the simulated annealing are presented in Table 2. They determine the initial and final temperatures T_i and T_f, as well as the number of cycles t_{iter} per temperature threshold and the cooling rate α.

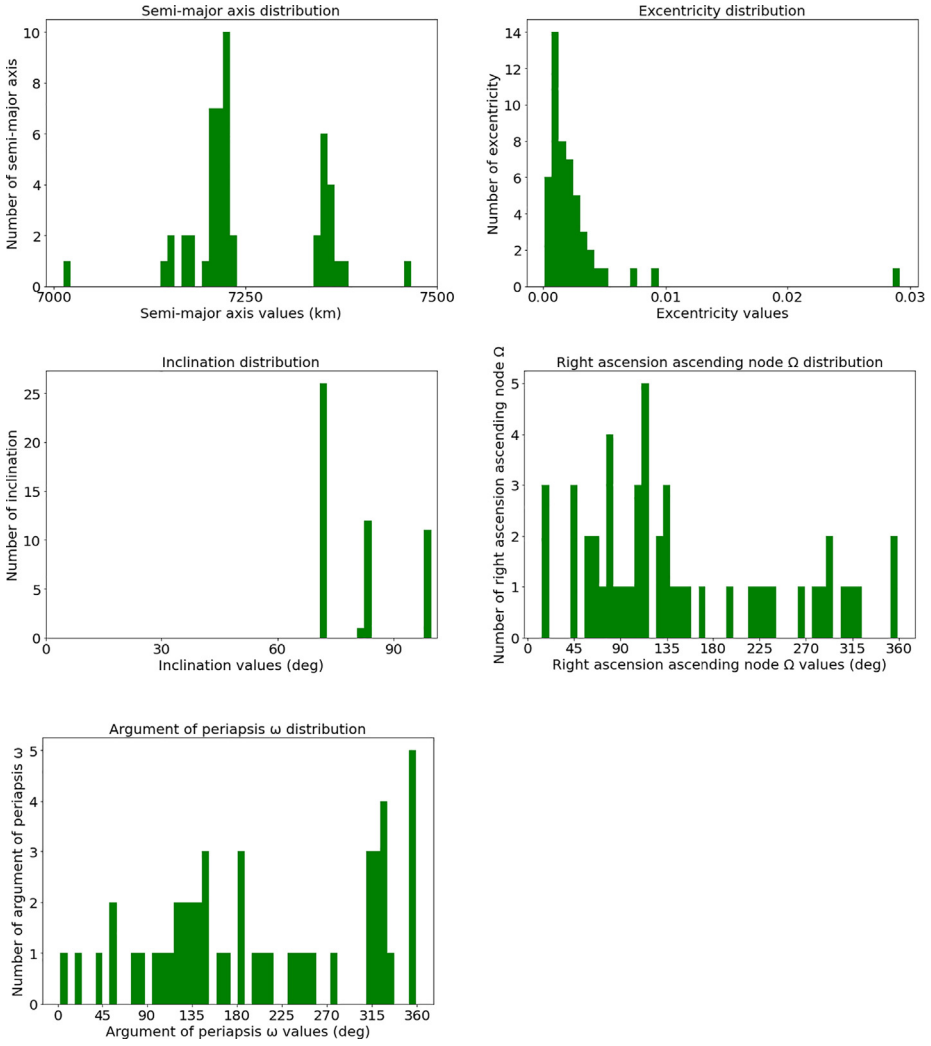

Fig. 9. Orbital parameters distribution for the 50 debris considered.

Table 1
Input parameters for ADR missions.

N_{debris}	ΔV_{max}	Δt_{max}	T_0
50	$4km.s^{-1}$	3 years	30th June 2022, 00:00

Table 2
Input parameters for simulated annealing.

T_i	T_f	t_{iter}	α
1.5	0.001	1000	0.95

The duration of an optimization with as parameterized here is about 3 h (Intel(R) Core(TM) i7-8700 CPU 3.2 GHz), and is about the same order of magnitude for each scenario. The number of iterations could be increased at the expense of the computation time in order to reach a global optimum, although the parameters used for this paper already seem to be sufficient. Thus, a simulation performed with a cooling rate $\alpha = 0.99$ runs for 16 h, and converges to the same solutions, as shown on Fig. 10.

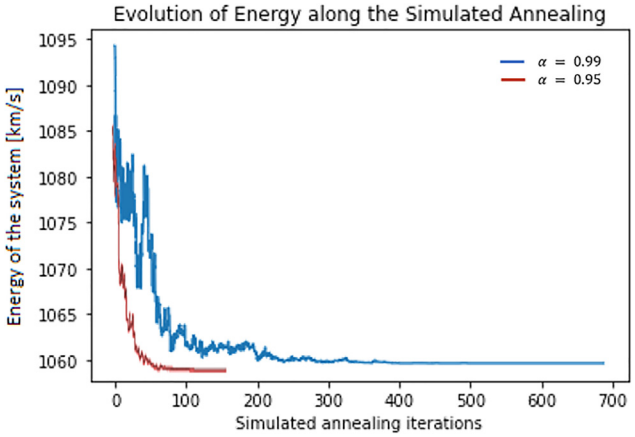

Fig. 10. Evolution of the energy of the system along the simulated annealing with $\alpha = 0.99$ and $\alpha = 0.95$.

6.3. ΔV and Δt matrix

The equations from (3)–(8) enable the calculation of the ΔV required to perform the transfer phases from debris k

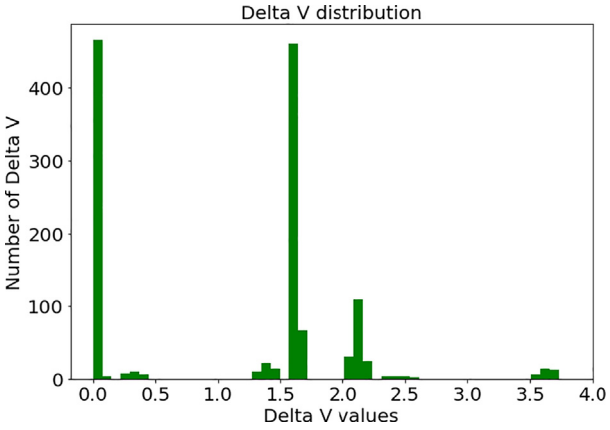

Fig. 11. ΔV distribution for scenario 1.

to debris l, for the 50 targeted debris. A distribution of these ΔV in a histogram is shown in Fig. 11 for scenario 1, where only the drift is used to align the Ω parameter, and the only maneuver performed is the alignment of the inclinations.

Several clusters emerge, with debris groups where very little ΔV is needed ($\Delta V < 0.5$ km/s) to perform the transfer: these are probably coplanar debris, where only a Hohmann transfer is needed. To perform a transfer to another group of debris with a different inclination, it is then necessary to perform a maneuver with at least a $\Delta V = 1.3$ km/s, some few transfers between two debris with very different orbits may require a $\Delta V = 3.5$ km/s, which is higher than desired.

As a reminder, we want an entire mission to require a $\Delta V < 3$ km/s. For this reason, we set the maximum ΔV value tolerated for a transfer to 2.5 km/s, and from the same equations we build a matrix representing the ΔV needed between two debris k and l, shown in Fig. 12, setting as a scale a maximum value $\Delta V = 2.5$ km/s.

As expected, three clusters with low ΔV emerge, corresponding to the distribution of debris at three inclinations seen in Fig. 9. It is also possible to make an associated Δt matrix applying the equations Eq. (10)–(12), with a maximum value of 1 year of transfer between each piece of debris, and presented in Fig. 13. The inputs (k, l) correspond to the drift time between debris k and l. It can be seen that these two matrices are complementary: the low ΔV clusters correspond to the clusters where the Δt is the highest, with a high time required to drift the Ω, while the high ΔV transfers are, in fact, quasi-instantaneous and correspond to reduced Δt values.

This complementarity of the matrices justifies the dual-objective approach needed to carry out an ADR mission, by bounding the trajectory optimization to both the cost in ΔV and the maximum duration of a mission.

If we built the same ΔV matrix for scenario 2 (Fig. 14), it can be seen, as expected, that performing all maneuvers, out-of-plane and in-plane, implies that all transfers require more than 2 km/s. Thus, almost all of the ΔV is in the Ω

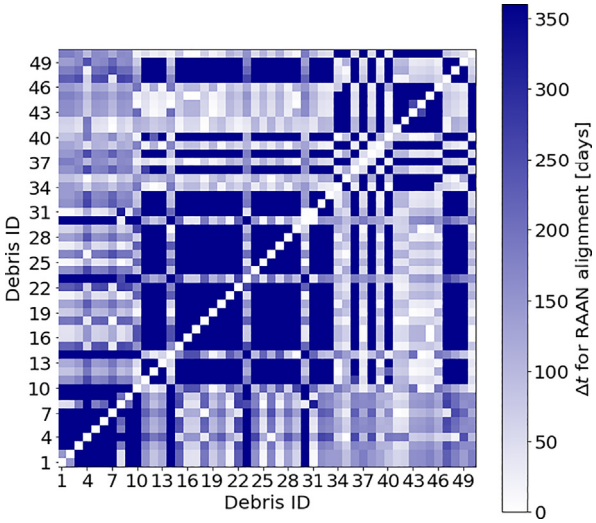

Fig. 13. Δt matrix for scenario 1 at t_0.

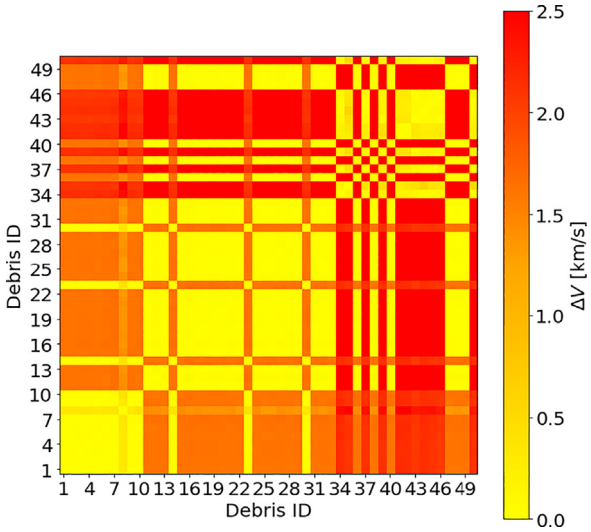

Fig. 12. ΔV matrix for scenario 1.

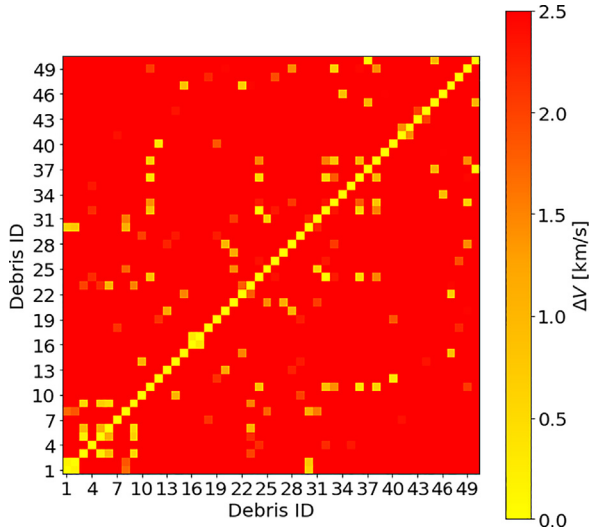

Fig. 14. ΔV matrix for scenario 2.

maneuver. Since the distribution in Ω is relatively uniform (similarly, see Fig. 9), there are no clusters of debris.

The application of scenario 3, which mixes maneuvers on Ω parameter and time drifts by weighting with a criterion, corresponds to applying either the ΔV calculated from the scenario 1 matrix (Fig. 12) or the ΔV calculated from the scenario 2 matrix (Fig. 14). These ΔV calculations are then used to determine the cost of a transfer between two debris k and l in the energy function.

It is then possible to make a ΔV matrix where the maneuvers in i and Ω are coupled, by applying Eq. (8), to reduce the cost in ΔV of an out-of-plane maneuver.

To better determine the influence of such a coupling, we remain within the framework of scenario 2, where each transfer between two pieces of debris k and l involves a maneuver in inclination and a maneuver in Ω. We subtract from the associated ΔV matrix, presented in Fig. 14, a new ΔV matrix where, this time, the i and Ω maneuvers, if any, are coupled for each transfer. The result of this difference is shown in Fig. 15, and corresponds to a ΔV difference.

The light green areas mean that the coupling did not result in any reduction in ΔV, and seem to correspond to the yellow areas in Fig. 12, which means that there is no i-maneuver. The coupling therefore brings no gain, since in both cases (with and without coupling), only the Ω maneuver is performed. On the contrary, the dark green areas mean that the coupling has allowed a strong reduction of the global ΔV, with the gain up to 4 km/s on the maneuver. This means that a maneuver was needed on both i and Ω, each requiring a considerable cost in ΔV, which the coupling allowed to reduce.

In fact, since the influence of coupling depends on the existence, or not, of a necessary maneuver on the inclination, it is consistent to find a distribution pattern similar to the one presented in Fig. 12, where the cost in ΔV also depended on the inclination difference.

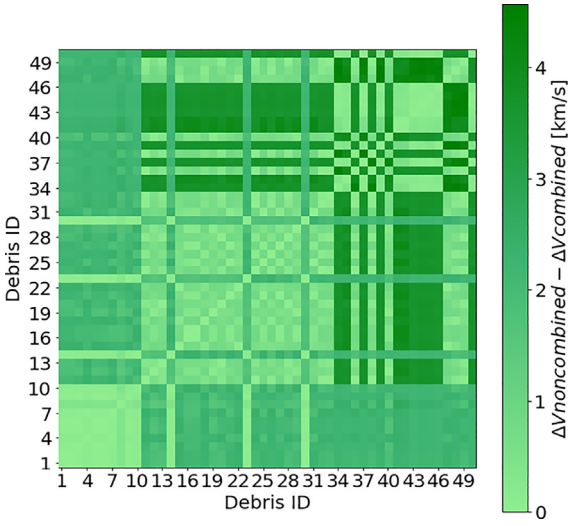

Fig. 15. Difference in ΔV for each transfer, between a transfer including two separate out-of-plane maneuvers, and a transfer where the maneuvers are coupled.

The conclusion of this study is that in the case of a double out-of-plane maneuver, it is meaningful to perform a coupled maneuver, in order to reduce the overall cost in ΔV, which makes the transfer between two pieces of debris less penalizing on the overall mission budget.

6.4. Optimal solutions according to the transfer scenarios

This section focuses on the comparison of the optimal solutions obtained when the 3 scenarios are applied, with the same parameters: the optimization parameters of the simulated annealing as well as the parameters of the global mission architecture are those presented in the Section 6.2. For scenario 2 and 3, the out-of-planes maneuvers are coupled. An additional study also presents the case of scenario 3 without coupling manoeuvers.

Scenario 1 proposes to maneuver a, i, and ω, and let the drift of J_2 operate to naturally modify Ω. The objective function E is set with $V_{tol} = 0$ km/s and $t_{tol} = 1$ year. The output results of the algorithm for scenario 1 are shown in Fig. 16, which gives, for each mission, the global cost in ΔV, in km/s, in red, and the global mission time Δt, in years, in green. This mission time includes drift time (when there is any), transfer time, phasing time and parking time. The overall average across all missions is shown as a dotted line.

The average number of debris per group is 4 ± 0.8, divided into 12 groups, with a minimum of 2 debris in group 6 and a maximum of 6 debris in group 10. The average ΔV cost is 3.45 ± 0.34 km/s, which is close to the maximum imposed limit of 4 km/s per mission. It is therefore the ΔV criterion which is restrictive in the objective function and which determines the distribution of the debris and the number of groups required.The average time spent on missions is quite scattered, with an average of $\Delta t = 2 \pm 0.71$ years. For the worst cases, the mission duration is 2.5 years, which is much longer than the recommendations from the simulations to remove about 5 pieces of debris per year. On the other hand, Group 6, with only two pieces of debris, has a short mission time of three

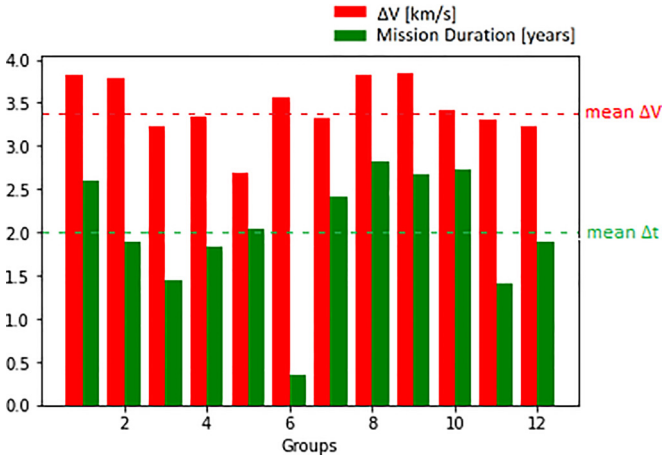

Fig. 16. ΔV and Δt budget per group for scenario 1.

and a half months, at a considerable cost in ΔV, at 3.45 ± 0.76 km/s.

Thus, as expected, the use of the drift in J_2 implies rather long mission durations, with exceptions, probably associated with a group of " outsiders ".

We therefore propose to check if it is not more advantageous in terms of Δt to carry out a maneuver directly on the RAAN: it is the scenario 2. In this case, the objective function E is set with $V_{tol} = 1$ km/s and $t_{tol} = 0$ year. Results from scenario 2 are presented in Fig. 17.

We can see that RAAN maneuvers, at least in our debris set, are extremely costly, as planned. In order to meet the maximum constraint of $\Delta V = 4$ km/s per mission, it is necessary to group the 50 pieces of debris into 16 groups, with an average of 3.1 ± 1.5 pieces of debris per group. The average ΔV for a mission is 2.4 ± 1.02km/s, while the average mission duration is 1.2 ± 0.9 years. Three groups, the n ° 9, 13 and 15, are made of one piece of debris, which explains why there is no ΔV or Δt associated with this group, as there is no transfer. On the other hand, the group 2, with the most debris, contains 6 pieces of debris.

Sending 16 ADR missions collecting only 3 pieces of debris on average each time, at considerable ΔV costs, is economically unsustainable given the prohibitive costs of launch, much less than scenario 1. However, the latter suffered from long mission times. We agree therefore that it is worthwhile to find a compromise with the drift due to the J_2. We propose to take advantage of the two previous scenarios, in order to create hybrid missions, in which the drift is used, but also maneuvers in RAAN. This leads to the scenario 3.

In the case of scenario 3, the results are compared for two cases: with and without coupling of the out-of-plane maneuvers (i, Ω). We assume to set $V_{tol} = 1km/s$ and $t_{tol} = 1year$, which was empirically found to be a good compromise. The same algorithm and mission architecture parameters than in Section 6.4 are applied.

In the case of coupled maneuvers, results in ΔV and Δt cost per mission are exposed in Fig. 18, while the details of the groups formed and the associated ΔV and Δt budget for each scenario can be found in Table 3. A binary RAAN manoeuvre vector is indicated in the table, such that: 0 means that no maneuver is performed, while 1 means that an out-of-plane maneuver has been performed.

These results show that the 50 pieces of debris can be deorbited by 12 ADR missions. The average number of debris per mission is 4.6, with one group consisting of a single piece of debris (Group 9), and one group consisting of 7 pieces of debris (Group 11). For the analysis of the results, it is assumed that the debris alone is not taken into account, since we wish to analyse the performance of multi-target missions.

Thus, out of the remaining 11 missions, the average cost in ΔV is 3.05 ± 0.48 km/s while the average mission time is 1.5 ± 0.4 years, which is well below the maximum criterion of 3 years and approaches the recommendations to remove about 5 pieces of debris per year. This corresponds to a number of missions similar to scenario 1, with the same number of debris per group on average, for a reduced ΔV cost and a reduced mission duration. The weighting between the out-of-plane maneuvers and the drift in J_2 thus improves the optimization of the groups compared to the use of the drift alone, and thus reduces the mission times (as expected), but also the overall ΔV , which is less expected, since an out-of-plane maneuver is added.

Thus, the highlighting of the transfers requiring maneuvers in Ω rather than drifting shows that some groups perform a maneuver for almost each transfer, without penalising the mass budget of the mission, which still comes to deorbit 5 pieces of debris. This is the case of the Groups 3, 5, 6, 11. This corresponds to very close orbits, where the correction in $\Delta\Omega$ is in the opposite direction than the direction of drift of the Ω, which implies a low cost in ΔV against a long time of drift Δt_{drift}. This case justifies the use of a mixed scenario to optimize the regrouping of debris without totally eliminating the possibility of carrying out a maneuver in Ω.

Then, a simulation is carried out with the same parameters, for the same scenario, without taking into account the coupling of maneuvers. The results are shown on Fig. 19. The 50 pieces of debris are divided this time into 14 ADR missions, with an average of 3.6 ± 1.2 pieces of

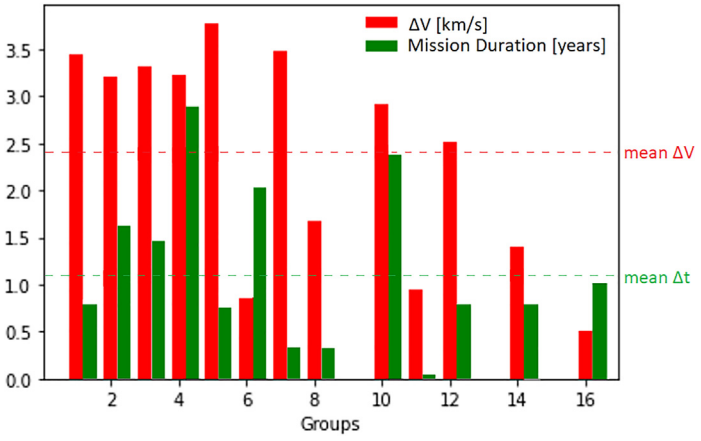

Fig. 17. ΔV and Δt budget per group for scenario 2.

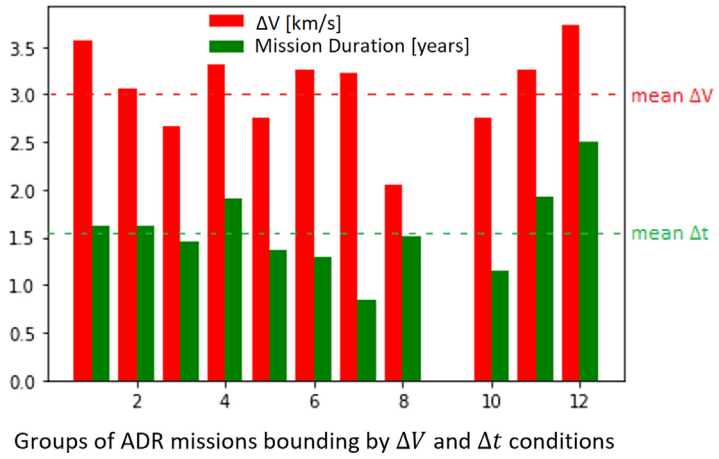

Fig. 18. ΔV and Δt per group for scenario 3.

Table 3
Group from scenario 3 with all $\Delta V < 4$ km/s and all $\Delta t < 3$ years.

Group	**1**	**2**	**3**	**4**
Debris	37, 1, 12, 34, 33	42, 6, 43, 45, 15	5, 18, 38, 22, 28	27, 8, 7, 48
Number of debris per group	5	5	5	4
ΔV (km/s)	3.56	3.04	2.66	3.31
Δt (years)	1.63	1.63	1.46	1.90
maneuver RAAN	(0, 0, 1, 0)	(1, 1, 0, 1)	(1, 1, 1, 1)	(0, 0, 0)
Group	**5**	**6**	**7**	**8**
Debris	11, 39, 4, 16	49, 30, 44, 24, 2	47, 29, 32	25, 9, 26, 20
Number of debris per group	4	5	3	4
ΔV (km/s)	2.75	3.26	3.23	2.04
Δt (years)	1.37	1.27	0.85	1.52
maneuver RAAN	(1, 1, 0)	(1, 1, 1, 0)	(0, 0)	(1, 0, 0)
Group	**9**	**10**	**11**	**12**
Debris	19	17, 3, 36	35, 10, 41, 23, 13, 40, 31	46, 21, 0, 14
Number of debris per group	1	3	7	4
ΔV (km/s)	0	2.76	3.26	3.74
Δt (years)	0	1.14	1.93	2.51
maneuver RAAN		(0, 1)	(1, 1, 1, 1, 1, 1)	(1, 0, 0)

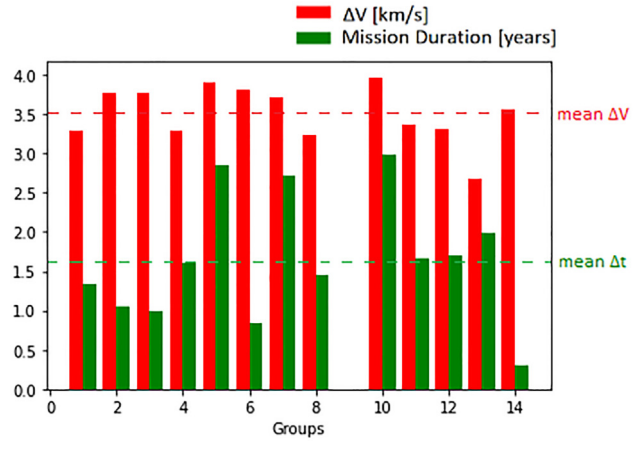

Fig. 19. ΔV and Δt per group for scenario 3 without combined maneuvers.

debris per mission, taking into account group 9 which has only one piece of debris. Without taking into account the 1-debris group, the average ΔV is 3.5 ± 0.4 km/s, and the average mission duration is 1.7 ± 0.8 years. It is noted that both averages are higher than in the previous case, where the maneuvers were coupled, even though the average number of pieces of debris, and therefore the number of transfers per mission, is lower. This simulation shows the huge benefits of combined maneuvers compared to the non-combined ones.

6.5. Optimal solutions with a debris limit per mission

As the average number of debris is 4, which is close to the 5 debris per mission recommended by the international agencies, a new simulation is carried out, where the mission architecture parameters are modified: the missions are no longer defined by a maximum cost in Δt and ΔV, but are defined by groupings of 4 to 5 debris. The results are shown on Fig. 20 and detailed in Table 4.

The number of ADR missions is reduced to 10 missions to deorbit the 50 pieces of debris, compared to the previous 11 missions to deorbit 49 pieces. The counterpart is an increase in the average ΔV, which is now 3.37 ± 0.3 km/s, and an increase in the average mission duration, which

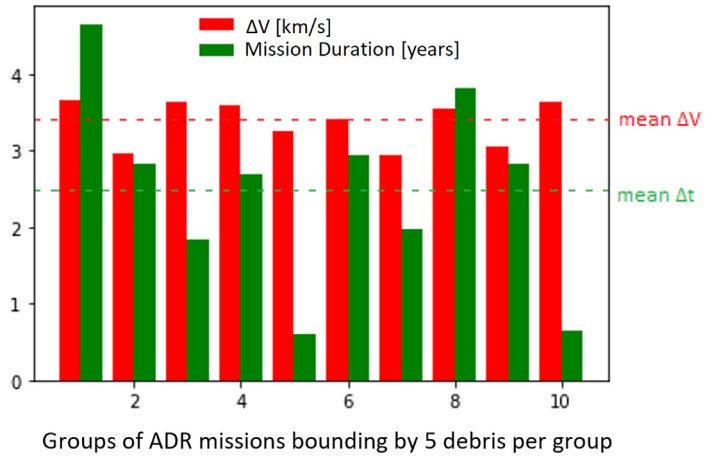

Fig. 20. ΔV and Δt per group for scenario 3, with a number of debris per groups sets between 4 and 5.

Table 4
Group from scenario 3 with a number of debris per groups sets between 4 and 5.

Group	**1**	**2**	**3**	**4**	**5**
Debris	40, 9, 25, 47, 31	17, 8, 48, 37, 27	33, 45, 43, 3, 18	28, 13, 44, 42, 49	12, 4, 7, 5, 14
Number of debris per group	5	5	5	5	5
ΔV (km/s)	3.66	2.96	3.64	3.59	3.27
Δt (years)	4.65	2.83	1.84	2.69	0.59
maneuver RAAN	(0, 0, 0, 0)	(0, 0, 0, 0)	(0, 0, 0, 0)	(0, 0, 0, 0)	(0, 0, 0, 0)
Group	**6**	**7**	**8**	**9**	**10**
Debris	11, 39, 29, 32, 35	10, 23, 22, 26, 24	19, 2, 38, 34, 36	30, 6, 16, 15, 20	41, 1, 0, 21, 46
Number of debris per group	5	5	5	5	5
ΔV (km/s)	3.39	2.95	3.55	3.05	3.65
Δt (years)	2.93	1.97	3.82	2.82	0.65
maneuver RAAN	(1, 0, 0, 0)	(0, 0, 0, 0)	(0, 0, 0, 0)	(0, 0, 0, 0)	(0, 0, 0, 0)

has risen to 2.5 ± 1.27 years per mission. There is therefore a huge disparity, particularly in terms of mission times, with some groups having a very low mission time, of the order of 7 months (groups 5 and 10), and others having a very high mission time, exceeding the initial 3-year criterion (groups 1 and 8). This disparity, linked to the absence of a criterion on the maximum tolerated duration of a mission, leads to another result: very few maneuvers are carried out on Ω, with only one listed. This means that the entire ΔV budget is consumed in inclination maneuvers and Hohmann transfers, and that the absence of RAAN maneuvers is compensated by the longer duration of missions. This is more or less the same as the values determined for scenario 1 when the missions were limited in budget and not in number of debris. This shows that constraining an ADR mission in terms of the number of debris items degrades the optimization of debris grouping.

This solution can be used if the predominant sizing criterion for the ADR mission is the number of kits to be transported per mission, rather than sizing on the maximum capacity of ΔV to be carried.

6.6. Discussion

The comparison of scenarios and mission criteria showed that the best debris cluster optimization occurs when the number of debris per mission is left free, and when a criterion is used to choose whether the correction of the Ω parameter is achieved by a maneuver or by natural alignment through orbit drift. In summary, the more flexible the tool, the better the optimization. So, we obtain average values of $\Delta V = 2.5$ km/s per mission, for an average duration of 1.5 years per mission. These values are higher than those found in the literature. However, the initial conditions are very different.

Thus, in (Cerf, 2015), the study aims to determine three missions of 5 debris to be removed from a list of 21 debris, with an inclination difference between the orbits of maximum 3°. The ΔV required to carry out these three missions is of the order of $830 m/s$ by chemical propulsion and 970 m/s by electric propulsion, with approximately 3 months of transfer between each piece of debris, i.e. a global mission time of $1.5 years$. These values in ΔV are much lower because almost only Hohmann transfers are performed, which is very cheap.

In (Zuiani and Vasile, 2012), the trajectory optimization is performed by minimising both the mission time and the ΔV cost, using a stochastic hybrid-memetic algorithm. 5 debris are predefined, with similar inclinations, with a maximum deviation of 4°. The test of all possible sequences between these 5 debris gives a ΔV between 2 and 2.5 km/s, for a mission duration between 3 months and 1.4 years,

in electric propulsion. This is therefore close to our values, while the inclination maneuvers are lower.

A similar study to ours is the one developed by (Carlo et al., 2017), where 25 pieces of debris are de-orbited by several electrically powered multi-target missions. The number of pieces of debris to be removed per mission is left open, and the optimization is performed by applying a physarium algorithm. These 25 pieces of debris are all located at the same inclination $i = 63°$, which removes all out-of-plane inclination correction maneuvers from the hybrid budget. The best optimization scenario then obtains a $\Delta V = 0.34$ km/s for a mission duration of 302 days, with the deorbiting of 9 to 10 objects per mission. The performance is therefore better than ours, but this is helped by an already optimized choice of debris to be removed. Indeed, if the inclinations are the same and the drift is used to align the RAANs, only Hohmann transfers are necessary, which explains the low cost in ΔV and the high debris removal capacity of a mission.

Another similar study is developed by ((Braun et al., 2013)), where the selected debris corresponds to dangerous debris, usually the second stages of launchers, as in our case. The inclination differences are therefore more pronounced, with i = 71°, 78° and 98°. In the case of chemical propulsion, 5 targets are removed at a cost of 7.5 km/s, and 4 targets are removed at a cost of 2.3 km/s, with each time a maneuver performed in i and also in Ω. The use of J_2 drift on debris of the same inclination reduces the ΔV budget to 1.2 km/s, for a 100-day mission. Thus, using a criterion that optimally choose between a RAAN natural drift and RAAN maneuver, we were able to stay within the same $\Delta V_{TOT} = 2.5$ km/s levels for deorbiting between 3 and 7 pieces of debris in one year and half, from a very unfavorable list.

A contrario, the list of debris selected for our use case is derived from real data, whose main selection criterion was the level of danger of the debris, without any consideration for its orbital parameters. Thus, our own orbital parameters are distributed in three main groups with high differences in inclination, with about 10° of inclination between each group, and with a RAAN distributed from 0° to 360°. This very unfavorable case in terms of trajectory optimization makes the maximum mission duration or the maximum propellant consumption tolerated more constraining, since it requires both very expensive out-of-plane maneuvers to gain degrees of inclination, and very long mission duration to align the spacecraft's RAAN with that of the following debris.

In spite of these higher constraints, the flexibility of our algorithm has enabled us to recover values approaching the high values of the literature, from much more unfavourable orbital parameters. This result also demonstrates the ability of our model to define groups of different debris sizes in order to obtain an equivalent ΔV_{TOT} from one mission to another, with similar mission times, from a list of 50 initial pieces of debris.

7. Conclusions and perspectives

Researching optimal debris groups to form deorbitation missions is a complex problem. The stochastic optimization process used, namely the Simulated Annealing, is capable of addressing this problem with a rather simple matrix formalism. The research work conducted has led to the development of a debris grouping and mission planning tool to optimize future multi-target ADR missions for any debris set. The tool, developed in Python, is fully customizable to best fit the mission requirements. Indeed, it remains possible to constrain the mission time, the ΔV budget, to modify the initial orbit of the satellite, to enlarge the debris list and to propose missions collecting more debris. Once the debris groups are formed, the tool proposes a mission architecture allowing the collect of all the debris of a group and guiding the user on the maneuvers to be done and their timing.

Thanks to the use of simulated annealing, which requires few parameters, the model can be applied whatever the number of debris, and the maximum mission duration can be modulated. The cases of application can therefore be very varied, depending on whether the mission architecture must favour long-duration missions (application of scenario 1 relying only on drift), or shorter-duration missions, or whether it is a question of servicing or removing debris. Furthermore, we showed that the overall cost in ΔV can be reduced by performing the out-of-plane maneuvers simultaneously, to correct the inclination and the RAAN (decoupled for the moment) at once.

However, this algorithm does not allow one to verify if the solution we have determined is indeed optimal. Moreover, the groups formed in the output are different from one optimization to the other, although they are extremely close in terms of minimized energy. However, this is understandable given the very large size of the research domain. Despite being the scenario with the largest research area, scenario number 3 seems to be the most promising in terms of ΔV and mission time trade-off.

There are several areas to explore in order to improve the tool we have developed. In the context of space mechanics, the mission duration can be reduced by placing the spacecraft on an intermediate orbit allowing the drift time of the RAAN to be reduced, by determining a trade-off between the necessary extra cost in ΔV compared to the gain in Δt_{drift}, as studied in (Cerf, 2013). The model can be completed by implementing the manoeuvres related to the orbital rendezvous, including the homing and closing phases. On the algorithmic side, an implementation of other optimization algorithms, such as ACO or GA, is planned in order to compare the performance of the different algorithms in terms of calculation speed and optimal solutions. In parallel, a parametric study on V_{tol} and t_{tol} will be conducted to determine the Pareto surface containing the most efficient solutions for the clusters formation. Similarly, a study on the weighting criterion between the maneuver in Ω and the drift in J_2 can be carried out, to adjust this parameter.

The application cases addressed by our solution are broad, and may generally concern ADR or IOS missions, regardless of the orbit (LEO, GEO, MEO). It can also be extended and adapted to the case of space exploration, visiting each exoplanet in a system once and only once, minimising propellant consumption and mission time.

Declaration of Competing Interest

The authors declare that they have no known competing financial interests or personal relationships that could have appeared to influence the work reported in this paper.

Acknowledgments

The authors would like to thank the Toulouse ISAE-SUPAERO engineering school for their resource commitment and technical contributions. In particular, the final year students who developed the optimization methodology and its implementation in an Active debris Removal Kit tool.

Appendix A. List of targeted debris

Fig. A.21 presents the list of the 50 statistically-most-concerning debris determined by the International Astronautical Federation, and used as database for our study. This list was constructed from several lists provided by international space agencies, including critical assumptions and key factors which give for each debris a "hazard score". It can be noted that these debris were all launched before the 2000s, when there was no concept of space debris management at all.

Ranking	Score	SATNO	Number of Lists	SATNAME	APOGEE, km	PERIGEE, km	INCL., deg	MASS, kg	COUNTRY	LAUNCH
1	4048	22,566	11	SL-16 R/B	848	837	71.0	9000	CIS	3/26/1993
2	3710	22,220	10	SL-16 R/B	848	827	71.0	9000	CIS	11/17/1992
3	3500	31,793	10	SL-16 R/B	846	843	71.0	9000	CIS	6/29/2007
4	3470	26,070	9	SL-16 R/B	854	827	71.0	9000	CIS	March 2, 2000
5	3330	16,182	10	SL-16 R/B	844	833	71.0	9000	CIS	10/22/1985
6	3300	20,625	10	SL-16 R/B	853	834	71.0	9000	CIS	5/22/1990
7	2880	27,006	8	SL-16 R/B	1006	986	99.5	9000	CIS	October 12, 2001
8	2862	23,705	9	SL-16 R/B	852	831	71.0	9000	CIS	10/31/1995
9	2826	25,407	9	SL-16 R/B	844	835	71.0	9000	CIS	7/28/1998
10	2800	23,405	10	SL-16 R/B	845	838	71.0	9000	CIS	11/24/1994
11	2547	17,974	9	SL-16 R/B	846	823	71.0	9000	CIS	5/13/1987
12	2412	23,088	8	SL-16 R/B	845	841	71.0	9000	CIS	4/23/1994
13	2296	22285	8	SL-16 R/B	844	840	71.0	9000	CIS	12/25/1992
14	2240	22,803	8	SL-16 R/B	850	823	71.0	9000	CIS	9/16/1993
15	1813	19,650	7	SL-16 R/B	848	831	71	9000	CIS	11/23/1988
16	1771	24,298	8	SL-16 R/B	863	839	70.8	9000	CIS	April 9, 1996
17	1650	28,353	7	SL-16 R/B	848	842	71.0	9000	CIS	October 6, 2004
18	1617	17,590	8	SL-16 R/B	841	831	71.0	9000	CIS	3/18/1987
19	1547	19,120	7	SL-16 R/B	842	814	71.0	9000	CIS	5/15/1988
20	1477	25,400	7	SL-16 R/B	813	801	98.6	9000	CIS	October 7, 1998
21	1320	27,386	5	ENVISAT	766	764	98.1	7800	ESA	January 3, 2002
22	1182	27,001	6	METEOR 3 M	1013	994	99.6	2500	CIS	October 12, 2001
23	805	24,277	4	ADEOS	794	793	98.9	3560	JPN	8/17/1996
24	600	27,601	4	H-2A R/B	836	734	98.2	3000	JPN	12/14/2002
25	564	15,334	4	SL-12 R/B(2)	847	838	71.0	2440	CIS	9/28/1984
26	512	37,932	4	CZ-2D R/B	846	791	98.7	4000	PRC	11/20/2011
27	468	10,732	4	SL-8 R/B	995	966	82.9	1435	CIS	3/15/1978
28	416	24,279	5	H-2 R/B	1306	860	98.7	2700	JPN	8/17/1996
29	384	23,704	3	COSMOS 2322	854	842	71.0	3250	CIS	10/31/1995
30	324	21,090	3	SL-8 R/B	992	961	82.9	1435	CIS	May 2, 1991
31	316	28,352	3	COSMOS 2406	863	844	71.0	3250	CIS	October 6, 2004
32	309	23,087	2	COSMOS 2278	852	841	71.1	3250	CIS	4/23/1994
33	270	19,119	2	COSMOS 1943	851	833	71.0	3250	CIS	5/15/1988
34	261	27,597	2	ADEOS 2	801	800	98.5	3680	JPN	12/14/2002
35	240	25,861	4	SL-16 R/B	645	622	98.2	9000	CIS	7/17/1999
36	240	15,772	3	SL-12 R/B(2)	848	794	71.1	2440	CIS	5/30/1985
37	228	10,693	3	SL-8 R/B	989	957	83.0	1435	CIS	2/28/1978
38	228	17,973	2	COSMOS 1844	866	824	71.0	3250	CIS	5/13/1987
39	225	27,387	3	ARIANE 5 R/B	796	748	98.6	2575	FR	January 3, 2002
40	207	7594	3	SL-8 R/B	981	955	82.9	1435	CIS	12/26/1974
41	207	23,180	3	SL-8 R/B	992	950	82.9	1435	CIS	7/14/1994
42	204	10,138	3	SL-8 R/B	1001	970	82.9	1435	CIS	August 7, 1977
43	204	13,917	3	SL-8 R/B	996	954	82.9	1435	CIS	3/24/1983
44	198	13,719	3	SL-3 R/B	896	791	81.3	1100	CIS	12/14/1982
45	194	14,625	2	SL-8 R/B	999	969	82.9	1435	CIS	November 1, 1984
46	183	20,624	2	COSMOS 2082	856	833	71.0	3250	CIS	5/22/1990
47	164	12,092	2	SL-8 R/B	996	953	82.9	1435	CIS	October 12, 1980
48	153	9044	3	SL-8 R/B	988	966	83.0	1435	CIS	7/21/1976
49	146	12,504	2	COSMOS 1275	1014	954	83.0	800	CIS	April 6, 1981
50	144	16,292	3	SL-8 R/B	996	953	82.9	1435	CIS	11/28/1985

Fig. A.21. List of 50 most dangerous debris according to the International Astronautical Federation.

References

Aglietti, G., Taylor, B., Fellowes, S., Ainley, S., Tye, D., Cox, C., Zarkesh, A., Mafficini, A., Vinkoff, N., Bashford, K., Salmon, T., Retat, I., Burgess, C., Hall, A., Chabot, T., Kanani, K., Pisseloup, A., Bernal, C., Chaumette, F., Pollini, A., Steyn, W., 2020. RemoveDEBRIS: An in-orbit demonstration of technologies for the removal of space debris. Aeronaut. J. 124 (1271), 1–23. https://doi.org/10.1017/aer.2019.136, URL: https://www.cambridge.org/core/product/identifier/S0001924019001362/type/journal_article.

Barbee, B.W., Alfano, S., Pinon, E., Gold, K., Gaylor, D., 2011. Design of spacecraft missions to remove multiple orbital debris objects. In: In 2011 Aerospace Conference. IEEE, Big Sky, USA, pp. 1–14. https://doi.org/10.1109/AERO.2011.5747303.

Black, A., Spencer, D.A., 2020. DragSail systems for satellite deorbit and targeted reentry. J. Space Saf. Eng. 7 (3), 397–403. https://doi.org/10.1016/j.jsse.2020.07.030, URL: https://linkinghub.elsevier.com/retrieve/pii/S2468896720300951.

Bombardelli, C., Pelaez, J., 2011. Ion beam shepherd for contactless space debris removal. J. Guidance, Control, Dyn. 34 (3), 916–920.

Botta, E.M., Sharf, I., Misra, A.K., 2019. Simulation of tether-nets for capture of space debris and small asteroids. Acta Astronaut. 155, 448–461. https://doi.org/10.1016/j.actaastro.2018.07.046, URL: https://linkinghub.elsevier.com/retrieve/pii/S0094576518303953.

Bourjolly, J.-M., Gurtuna, O., Lyngvi, A., 2006. On-orbit servicing: a time-dependent, moving-target traveling salesman problem. Int. Trans. Oper. Res. 13 (5), 461–481, URL https://onlinelibrary.wiley.com/doi/10.1111/j.1475-3995.2006.00558.x.

Braun, V., Lüpken, A., Flegel, S., Gelhaus, J., Möckel, M., Kebschull, C., Wiedemann, C., Vörsmann, P., 2013. Active debris removal of multiple priority targets. Adv. Space Res. 51 (9), 1638–1648. https://doi.org/10.1016/j.asr.2012.12.003, URL: https://linkinghub.elsevier.com/retrieve/pii/S0273117712007399.

Busetti, F., 2001. Simulated annealing overview. URL: https://www.researchgate.net/publication/238690391_Simulated_annealing_overview.

Cercos, L., Stefanescu, R., Medina, A., Benvenuto, R., Lavagna, M., Gonzalez, I., Rodriguez, N., Wormnes, K., 2014. Validation of a Net Active Debris Removal simulator within parabolic flight experiment. Archivio istituzionale della ricerca - Politecnico di Milano, pp. 1–8.

Cerf, M., 2013. Multiple Space Debris Collecting Mission—Debris Selection and Trajectory Optimization. J. Optim. Theory Appl. 156 (3), 761–796. https://doi.org/10.1007/s10957-012-0130-6, URL: http://link.springer.com/10.1007/s10957-012-0130-6.

Cerf, M., 2015. Multiple space debris collecting mission: optimal mission planning. J. Optim. Theory Appl. 167 (1), 195–218. https://doi.org/10.1007/s10957-015-0705-0, URL: http://link.springer.com/10.1007/s10957-015-0705-0.

Chmait, N., Challita, K., 2013. Using simulated annealing and ant-colony optimization algorithms to solve the scheduling problem. csit 1 (3), 208–224. https://doi.org/10.13189/csit.2013.010307, URL: http://www.hrpub.org/journals/article_info.php?aid=671.

Colmenarejo, P., Binet, G., Strippoli, L., Peters, T.V., Graziano, M., 2012. GNC Aspects for Active Debris Removal. Proceedings of the EuroGNC 2013, 2nd CEAS Specialist Conference on Guidance, Navigation & Control, p. 19.

Colombo, C., Rossi, A., Vedova, F.D., Braun, V., BastidaVirgili, B., Krag, H., 2017. Drag and solar sail deorbiting: re-entry time versus cumulative collision probability. In: 68th International Astronautical Congress, p. 19.

Di Carlo, M., Romero Martin, J.M., Vasile, M., 2017. Automatic trajectory planning for low-thrust active removal mission in low-earth orbit. Adv. Space Res. 59 (5), 1234–1258. https://doi.org/10.1016/j.asr.2016.11.033, URL: https://linkinghub.elsevier.com/retrieve/pii/S0273117716306767.

Dudziak, R., Tuttle, S., Barraclough, S., 2015. Harpoon technology development for the active removal of space debris. Adv. Space Res. 56 (3), 509–527. https://doi.org/10.1016/j.asr.2015.04.012, URL: https://linkinghub.elsevier.com/retrieve/pii/S0273117715002719.

Federici, L., Zavoli, A., Colasurdo, G., 2019. A Time-Dependent TSP formulation for the design of an active debris removal mission using simulated annealing. Adv. Astronaut. Sci. 171. URL: http://arxiv.org/abs/1909.10427. ArXiv: 1909.10427.

Han, C., Zhang, S., Wang, X., 2019. On-orbit servicing of geosynchronous satellites based on low-thrust transfers considering perturbations. Acta Astronaut. 159, 658–675. https://doi.org/10.1016/j.actaastro.2019.01.041, URL: https://linkinghub.elsevier.com/retrieve/pii/S0094576518319799.

Gauss, C.F., 1864. Theoria motus cœlestium in sectionibus conicis solem ambientium (Theory of motion of celestial bodies travelling in conical sections around the sun). Edmond Dubois. URL: https://www.gabay-editeur.com/GAUSS-Theorie-du-mouvement-des-corps-celestes-1864.

Inter-agency Space Debris Coordination Committee, 2002. IADC space debris mitigation guidelines. UN COPUOS 40th session, Vienna.

Izzo, D., Getzner, I., Hennes, D., Simões, L.F., 2015. Evolving Solutions to TSP Variants for Active Space Debris Removal. In: Proceedings of the 2015 Annual Conference on Genetic and Evolutionary Computation, Madrid Spain: ACM, pp. 1207–1214. URL: https://dl.acm.org/doi/10.1145/2739480.2754727. https://doi.org/10.1145/2739480.2754727.

Izzo, D., Luís F., S., 2018. Acta Futura, Issue 11. Zenodo. URL: https://zenodo.org/record/1142857. https://doi.org/10.5281/ZENODO.1142857.

Kanazaki, M., Yamada, Y., Nakamiya, M., 2018. Multi-objective path optimization of a satellite for multiple active space debris removal based on a method for the travelling serviceman problem. Adv. Sci. Technol. Eng. Syst. J. 3 (6), 479–488, URL https://astesj.com/v03/i06/p56/.

Kessler, D.J., Cour-Palais, B.G., 1978. Collision frequency of artificial satellites: The creation of a debris belt. J. Geophys. Res. 83 (A6), 26–37.

Kirkpatrick, S., Gelatt, C., Vecchi, M., 1983. Optimization by simulated annealing. Science (New York, N.Y.), 220, pp. 671–680. https://doi.org/10.1126/science.220.4598.671.

Kitamura, S., Hayakawa, Y., Kawamoto, S., 2011. A Reorbiter for GEO Large Space Debris Using Ion Beam Irradiation. In: Presented at the 32nd International Electric Propulsion Conference, Wiesbaden, Germany.

Lavagna, M.R., Armellin, R., Bombelli, A., Benvenuto, R., Carta, R., 2012. Debris removal mechanism based on tethered nets: I-SAIRAS 2012. In: Proceedings of the 11th International Symposium on Artificial Intelligence, Robotics and Automation in Space, i-SAIRAS 2012, pp. 1–7.

Lewis, H.G., White, A.E., Crowther, R., Stokes, H., 2012. Synergy of debris mitigation and removal. Acta Astronaut. 81 (1), 62–68.

McKnight, D., Witner, R., Letizia, F., Lemmens, S., Anselmo, L., Pardini, C., Rossi, A., Kunstadter, C., Kawamoto, S., Aslanov, V., Dolado Perez, J.-C., Ruch, V., Lewis, H., Nicolls, M., Jing, L., Dan, S., Dongfang, W., Baranov, A., Grishko, D., 2021. Identifying the 50 statistically-most-concerning derelict objects in LEO. Acta Astronaut. 181, 282–291. https://doi.org/10.1016/j.actaastro.2021.01.021, URL: https://linkinghub.elsevier.com/retrieve/pii/S0094576521000217.

Merz, K., Virgili, B.B., Braun, V., Flohrer, T., Funke, Q., Krag, H., Lemmens, S., 2017. Current Collision Avoidance service by ESA's Space Debris Office. Proc. In: 7th European Conference on Space Debris, p. 11.

Miettinen, K., Mäkelä, M.M., 2002. On scalarizing functions in multiobjective optimization. OR Spectrum. 24 (2), 193–213. https://doi.org/10.1007/s00291-001-0092-9, URL: http://link.springer.com/10.1007/s00291-001-0092-9.

Nowakowski, P., Kasztankiewicz, A., Marciniak, B., Okninski, A., Pakosz, M., Noga, T., Majewska, E., Rysak, D., Wolanski, P., 2019. Space Debris Mitigation using dedicated Solid Rocket Motor. 8TH european conference for aeronautics and space sciences (EUCASS), p. 10 pages. URL: https://www.eucass.eu/doi/EUCASS2019-0994.pdf.

https://doi.org/10.13009/EUCASS2019-994. Artwork Size: 10 pages Medium: PDF Publisher: Proceedings of the 8th European Conference for Aeronautics and Space Sciences. Madrid, Spain, 1-4 July 2019.

Sizov, D.A., Aslanov, V.S., 2021. Space debris removal with harpoon assistance: choice of parameters and optimization. J. Guidance, Control, Dyn. 44 (4), 767–778. https://doi.org/10.2514/1.G005484, URL: https://arc.aiaa.org/doi/10.2514/1.G005484.

Wiedemann, C., Flegel, S., Möckel, M., Gelhaus, J., Braun, V., Kebschull, C., Kreisel, J., Metz, M., Vörsmann, P., 2013. The economics of the controle of the space debris environment. In: Proc. 6th European Conference on Space Debris, p. 8.

Yakovlev, M., 2005. The "IADC Space Debris Mitigation Guidelines" and Supporting Documents. In: Danesy, D. (Ed.), 4th European Conference on Space Debris, vol. 587. ESA Special Publication, p. 591.

Zhang, H., Ge, H., Yang, J., Tong, Y., 2022. Review of Vehicle Routing Problems: Models, Classification and Solving Algorithms. Arch. Comput. Methods Eng.: State Art Rev. 29(1), 195–221. URL: https://search.ebscohost.com/login.aspx?direct=true&db=edssjs&AN=edssjs.85A677F9&site=eds-live. https://doi.org/10.1007/s11831-021-09574-x. Place: Dordrecht Publisher: Springer, Netherlands.

Zuiani, F., Vasile, M., 2012. Preliminary design of debris removal missions by means of simplified models for low-thrust, many-revolution transfers. Int. J. Aerospace Eng., 2012, 1–22. URL: http://www.hindawi.com/journals/ijae/2012/836250/. https://doi.org/10.1155/2012/836250.

Shirazi, A., Ceberio, J., & Lozano, J. A. (2018). Spacecraft trajectory optimization: A review of models, objectives, approaches and solutions. Progress in Aerospace Sciences, 102, 76–98. URL: https://linkinghub.elsevier.com/retrieve/pii/S0376042118300198. doi:10.1016/j.paerosci.2018.07.007.